© 2024. Published by The Company of Biologists Ltd | Journal of Experimental Biology (2024) 227, jeb246879. doi:10.1242/jeb.246879

RESEARCH ARTICLE

Linking *in vivo* muscle dynamics to force–length and force–velocity properties reveals that guinea fowl lateral gastrocnemius operates at shorter than optimal lengths

M. Janneke Schwaner[1,*], Dean L. Mayfield[1,2], Emanuel Azizi[1] and Monica A. Daley[1,3]

ABSTRACT

The isometric force–length (*F–L*) and isotonic force–velocity (*F–V*) relationships characterize the contractile properties of skeletal muscle under controlled conditions, yet it remains unclear how these properties relate to *in vivo* muscle function. Here, we map the *in situ F–L* and *F–V* characteristics of guinea fowl (*Numida meleagris*) lateral gastrocnemius (LG) to the *in vivo* operating range during walking and running. We test the hypothesis that muscle fascicles operate on the *F–L* plateau, near the optimal length for force (L_0) and near velocities that maximize power output (V_{opt}) during walking and running. We found that *in vivo* LG velocities are consistent with optimizing power during work production, and economy of force at higher loads. However, LG does not operate near L_0 at higher loads. LG length was near L_0 at the time of electromyography (EMG) onset but shortened rapidly such that force development during stance occurred on the ascending limb of the *F–L* curve, around $0.8L_0$. Shortening across L_0 in late swing might optimize potential for rapid force development near the swing–stance transition, providing resistance to unexpected perturbations that require rapid force development. We also found evidence of *in vivo* passive force rise in late swing, without EMG activity, at lengths where *in situ* passive force is zero, suggesting that dynamic viscoelastic effects contribute to *in vivo* force development. Comparison of *in vivo* operating ranges with *F–L* and *F–V* properties suggests the need for new approaches to characterize muscle properties in controlled conditions that more closely resemble *in vivo* dynamics.

KEY WORDS: Muscle function, Muscle physiology, Work loop, Work loops, Muscle properties

INTRODUCTION

The isometric force–length (*F–L*) and isotonic force–velocity (*F–V*) relationships are two widely used empirical measures of muscle contractile properties that characterize mechanical output under controlled conditions (Blix, 1894; Hill, 1938; Gordon et al., 1966; Huxley, 1957; Caiozzo, 2002; Nelson et al., 2004; Alcazar et al., 2019; Sugi and Ohno, 2019). The most common purpose of *F–L* and *F–V* experiments is to systematically characterize muscle contractile properties under consistent conditions that can be compared across fiber types, muscles, species and experimental treatment groups (e.g. changes with training, unloading, age, drug treatment, etc.) (Always, 1995; Rassier et al., 1999; Jones, 2010; Raj et al., 2010). The *F–L* relationship identifies the fascicle length associated with maximum isometric force (L_0), and the *F–V* relationship demonstrates the force–velocity trade-off that results in an optimal velocity for maximum power output (V_{opt}) (e.g. Fenn and Marsh, 1935; Gordon et al., 1966; James et al., 1998; Zajac, 1989; Askew and Marsh, 1998). These characteristics are often used to interpret *in vivo* muscle fascicle lengths, velocities and forces. These properties are also widely used to specify Hill-type muscle actuator properties in musculoskeletal and neuromechanical simulations of movement, in software such as OpenSim and AnyBody (e.g. Delp et al., 2007; Biewener et al., 2014; Seth et al., 2018; Cox et al., 2019). However, the tightly controlled experimental conditions resulting in the *F–L* and *F–V* relationships do not represent typical *in vivo* conditions, which are submaximal and include dynamic, time-varying activation, force, length and velocity. Some previous studies have compared *in vivo* operating lengths with the *F–L* curve, but most of these studies focused on *in vivo* strain ranges, without direct measures of muscle force (e.g. Gregor et al., 1988; Holt and Azizi, 2014; Ahn et al., 2018). Considering the wide-spread use of *F–L* and *F–V* properties to characterize muscle contractile performance, it is important to understand how these properties relate to *in vivo* muscle fascicle operating ranges and force and power output.

With *in vivo* muscle fascicle strain and muscle–tendon force data, work loops can characterize muscle mechanical function under dynamic *in vivo* conditions (Josephson, 1985; Prilutsky et al., 1996; Roberts et al., 1997; Biewener et al., 1998a,b; Roberts, 2001; Ahn, 2012; Sawicki et al., 2015; Sponberg et al., 2023). By plotting force against length over a full cycle, the area enclosed by the force–length loop corresponds to the total work output of the muscle and is therefore called a 'work loop'. *In vivo* work loops can characterize the complexity and variation in function of muscles in natural movements, with time-varying activation, strain and force. These work loops can have complex shapes, due to less constrained length and activation trajectories compared with the sinusoidal trajectories typically used for *ex vivo* or *in situ* work loops (Tu and Dickinson, 1994; Luiker and Stevens, 1994; Stevens, 1996; Rome and Lindstedt, 1997; Askew and Marsh, 1997). For example, *in vivo* work loops in turkeys and wallabies have revealed that some distal muscles with long in-series tendons contract isometrically during force development in steady locomotion, resulting in an L-shaped work loop representing a 'strut-like' function, which enables tendinous structures to cycle elastic energy (Roberts et al., 1997; Biewener et al., 1998b; Griffiths, 1989). *In vivo* studies have also revealed that work loop shape is sensitive to the load applied during early muscle activation, as well as the phase of activation relative to the applied load (Daley and Biewener, 2003; Daley et al., 2009;

[1]Department of Ecology and Evolutionary Biology, University of California, Irvine, Irvine, CA 92697, USA. [2]Department of Evolution, Ecology, and Organismal Biology, University of California, Riverside, Riverside, CA 92521, USA. [3]Center for Integrative Movement Sciences, University of California, Irvine, Irvine, CA 92617, USA.

*Author for correspondence (mariejanneke.schwaner@kuleuven.be)

M.J., 0000-0002-1666-3111; M.A.D., 0000-0001-8584-2052

Received 11 October 2023; Accepted 10 June 2024

Daley and Biewener, 2011; Gordon et al., 2020; Schwaner et al., 2023). For example, during strenuous locomotor tasks, such as incline running or obstacle navigation, the LG shows a more open work loop compared with steady, level locomotion, as a result of earlier force onset at longer muscle fascicle lengths (Roberts et al., 1997; Daley and Biewener, 2003, 2011; Daley et al., 2009; Gordon et al., 2020; Schwaner et al., 2023). While these *in vivo* studies provide insight into the functional range of muscle and the dynamic interactions between strain, activation and force, it can be difficult to interpret underlying mechanisms because of the complexity and variability of *in vivo* data. Consequently, it is important to connect contractile mechanisms measured through controlled benchtop experiments (*ex vivo*, *in situ*), to the more realistic and complex conditions of *in vivo* natural movements (Sponberg et al., 2023).

The experimental conditions for the *F–L* and *F–V* curves differ from *in vivo* contraction conditions because they are tightly controlled to keep length and tension constant, respectively. *In vivo* muscle fascicle length trajectories are dynamic, and force output varies depending on both activation and strain history (Josephson, 1999; Edman et al., 1982; Gregor et al., 1988; Herzog et al., 1992). Additionally, while passive forces are approximated as exponential in the *F–L* curve, in reality, passive forces are also time and history dependent, and will therefore vary under dynamic conditions (Joumaa et al., 2008; Herzog, 2019). Furthermore, both the *F–L* and *F–V* relationships are typically collected under maximal stimulation, which rarely occurs *in vivo* (Strojnik, 1995). Under submaximal conditions, the plateau of the *F–L* curve shifts to longer lengths with decreasing activation level, and the *F–V* curve shifts to lower forces for a given shortening velocity (de Haan, 1988; Chow and Darling, 1999; Holt and Azizi, 2014, 2016; Holt et al., 2014). These differences have important implications for interpreting *in vivo* operating ranges relative to inferred maximal capacities for force, power and shortening velocity. For example, during maximum jumping tasks, cane toads and frogs shorten their muscle fascicles across the *F–L* plateau, operating their muscle fascicles around L_0 and V_{opt} (i.e. Holt and Azizi, 2016). However, for lower jump distances, with lower activation, *in vivo* operating ranges are poorly aligned with optimal lengths and velocities predicted by the maximal tetantic *F–L* and *F–V* curves (Holt and Azizi, 2016). Previous studies have focused on quantifying muscle operating length for near-maximum ballistic behaviors (Azizi and Roberts, 2010), and fewer have analyzed muscle force and operating lengths during submaximal cyclical tasks (Gregor et al., 1988; Rubenson et al., 2012; Bohm et al., 2019). Therefore, it is still largely unknown how *F–L* and *F–V* muscle properties relate to *in vivo* muscle fascicle operating ranges during submaximal locomotion.

Here, we investigated the correspondence between muscle *F–L* and *F–V* relationships and the *in vivo* muscle dynamics and operating ranges in the guinea fowl lateral gastrocnemius (LG) muscle during walking and running. We compared LG *F–L* and *F–V* characteristics across individuals, and directly related an individual's *in vivo* work loop during walking and running to their respective *F–L* and *F–V* characteristics, to evaluate muscle contraction dynamics over complete stride cycles. Long-standing arguments suggest that muscle fascicles operate near optimal conditions for force and power during *in vivo* tasks (Rome, 1998; Burkholder and Lieber, 2001; Lieber and Ward, 2011). Here, we tested the hypothesis that muscle fascicles operate on the *F–L* plateau, near L_0 to optimize economy of force development, and at velocities near V_{opt} to optimize power production during walking and running. Previous work revealed that the LG produces work while rapidly shortening under low forces around the swing–stance transition, and then rapidly transitions to near-isometric contraction just after the time of foot contact (T_c), acting as a strut as forces reach a peak around mid-stance (Daley and Biewener, 2003, 2011; Gordon et al., 2020; Schwaner et al., 2023). Therefore, we expected LG to operate near V_{opt} while producing work during the swing–stance transition, and to operate near zero velocity and L_0 at the time of peak force for economy of force development. Additionally, we aimed to fully characterize LG operating range during walking and running and evaluate dynamic relationships between strain and force observed *in vivo*. We tested for a correlation between *in situ* connective tissue compliance and work loop shape, to determine whether individuals with higher compliance exhibit higher *in vivo* muscle work output during walking and running. Data relating *in situ* and *in vivo* muscle properties are essential to understand contributors to *in vivo* force development beyond the *F–L* and *F–V* properties, and to inform future benchtop experiments that characterize muscle under controlled yet dynamic conditions that more accurately reflect natural movements.

MATERIALS AND METHODS

Animals

We used 11 adult guinea fowl, *Numida meleagris* (Linnaeus 1758), for this study. We divided animals into two cohorts: combined *in vivo* and *in situ* (n=6) and *in situ* only (n=5). The combined *in vivo* and *in situ* birds were habituated to handling and trained on the treadmill before treadmill data collection sessions. These birds first underwent surgical procedures for *in vivo* transducer implantation, and *in vivo* data collection while walking and running on the treadmill, before collection of *in situ* data. The details of the procedures are described below. The *in situ* only cohort was used as a quality control to ensure that *in situ* data collected following *in vivo* experiments were similar to data collected without a prior *in vivo* procedure. All procedures were licensed and approved by the University of California Institutional Animal Care and Use Committee (IACUC) (AUP 20-048). Animals were euthanized at the end of the experiments by injection of Euthasol (pentobarbital sodium) while under deep isoflurane anesthesia (5%) delivered by mask.

In vivo transducer implantation

Sonomicrometry, electromyography (EMG) and force transducers were implanted into the LG muscle and its associated distal tendon while the animals were under surgical anesthesia (isoflurane 1.5–3%, mask delivery), following procedures similar to Daley and Biewener (2003, 2011). Feathers were removed from the left leg, and the surgical field was cleaned 3 times with antiseptic solution (povidone iodine) and alcohol wipes. Transducer leads were tunneled under the skin from a ∼20 mm incision over the synsacrum to a ∼50 mm incision over the lateral shank. Sonomicrometry crystals (1.0 mm; Sonometrics Inc., London, ON, Canada) were implanted within the LG muscle belly in the middle third of the muscle, aligned along muscle fascicles. The alignment of crystals was checked post-mortem to ensure that fascicle lengths were measured accurately. Transducer signals from a sonometrics DS3 digital sonomicrometer (Sonometrics Inc.) were checked via SonoLab software (Sonometrics Inc.). Transducers were secured and the muscle was closed using 5-0 silk suture (Silk, Ethicon, Somerville, NJ, USA). Two bipolar EMG electrodes (AS 632 Teflon-coated stainless steel wire, Cooner Wire Co., Chatsworth, CA, USA) were implanted in the middle third of the muscle belly. A custom-designed E-type stainless steel tendon buckle force transducer was placed around the common gastrocnemius tendon and secured with 5-0 silk ties. EMG and buckle transducers were connected through a 9-way micro-connector plug (580-M09,

NorComp Inc., Charlotte, NC, USA). Sonomicrometry leads were connected through an 18-way connector [ST60-18P(30), Hirose Electric Co. Ltd, Downers Grove, IL, USA]. Both connectors were secured using 4-0 silk suture to the skin on the bird's dorsal synsacrum. Skin was closed using 4-0 silk suture (Silk, Ethicon). At the end of the surgery, joint centers of rotation were marked using a combination of permanent markers (black medium sharpie, Newell-Rubbermaid Office, Oak Brook, IL, USA) and non-toxic paint (Painters, Elmer's Products Inc., Westerville, OH, USA).

In vivo data collection

As part of a larger study, we recorded steady-state locomotion trials that were each 30 s in duration, for a total of 4–12 trials per individual over 1–3 days of experiments (2–6 trials per day) (Schwaner et al., 2022). Birds walked and ran on a motorized treadmill (Woodway, Waukesha, WI, USA) at constant speeds of 0.67 and 1.56 m s^{-1}, respectively. We recorded *in vivo* EMG, muscle fascicle length changes and muscle tendon force at 5000 Hz using the USB-6363-X model National Instruments Data Acquisition board through the MATLAB data acquisition toolbox (Analog Input Recorder Application, MATLAB 2021a, MathWorks, Natick, MA, USA). We recorded video from the sagittal plane using a high-speed camera (collected at 200 Hz, Phantom VEO 410S, Wayne, NJ, USA). For each bird, we selected one trial per gait condition (i.e. walking and running) for further analysis. We selected the trial in which the bird maintained steady speed for most of the trial and we had a complete dataset for the entire trial, including video, muscle force, muscle fascicle length and EMG activity data.

In vivo data analysis

The joint centers of rotation and several body points were digitized using DeepLabCut (version 2.2.1) (Mathis et al., 2018; Nath et al., 2019) (see Schwaner et al., 2022). Filtered marker locations (low-pass second-order Butterworth filter, cut-off frequency of 30 Hz) were used to determine foot contact and take-off times and ankle joint kinematics. We tracked stance, swing and stride periods based on foot contact and take-off times using the kinematics of the instrumented left leg, after Schwaner et al. (2022). Using the ankle joint kinematics, we cut strides from mid-swing to mid-swing. Unsteady strides resulting from accelerations, decelerations or unexpected animal movement were excluded from analysis. Steady strides were determined based on foot velocity during stance being within 3 s.d. of the treadmill belt speed. We further analyzed *in vivo* measures of muscle force, fascicle length, activation and kinematics in a custom-written MATLAB script (MATLAB, version 2021a, MathWorks). We obtained myoelectric intensities from raw EMG signals in time and frequency using wavelet decomposition, using wavelets optimized for muscle (after Von Tscharner, 2000; Wakeling et al., 2002; Daley et al., 2009; Gordon et al., 2015; Schwaner et al., 2023). We calculated an activation threshold as +3 s.d. above baseline muscle activation, and used these to determine the onset and offset timing of muscle activation (T_{act}, T_{deact}, respectively) for further analysis. To characterize *in vivo* fascicle length and velocity operating ranges, we identified five important time points during the stride cycle for further analysis: (1) time of LG EMG activity onset (T_{act}), (2) time of foot contact (T_c), (3) time of 50% force rise (T_{rise}), (4) time of peak force (T_{peak}) and (5) time of 50% force decay (T_{fall}).

In situ data collection

For all individuals (n=11), we characterized the *F–L* and *F–V* relationships *in situ*. Birds were maintained under deep surgical anesthesia throughout the experiment (induction at 2.5–3% isoflurane, maintenance at 1.5–2%, mask delivery). A ∼25 mm incision was made posterior to the thigh muscles to access the sciatic nerve, which was isolated and instrumented with a custom-built nerve cuff (after Naples et al., 1988) and then immersed in mineral oil. For *in situ* only birds, the left LG muscle was instrumented with sonomicrometry transducers (1.0 mm, Sonometrics Inc.), positioned mid-belly along the fascicle, in the same position as for the *in vivo* birds. For the *in vivo* birds, we used the sonomicrometry crystals already placed in the previous surgery. The distal free tendon of the gastrocnemius muscle was connected to an ergometer (310C-LR, Aurora Scientific Inc., Aurora, ON, Canada) using a custom clamp allowing measurement of muscle force and changes in muscle length. On average, 20.8±6.6 mm free tendon (mean±s.d.) remained attached to the muscle during experiments. The clamp was placed immediately proximal to the extra cartilaginous tissue that occurs in the tendon at the crossing of the ankle joint, while avoiding the force buckle. The medial gastrocnemius (MG) was separated from the LG by making an incision along the aponeurosis connective tissue between the two muscles.

For combined *in vivo* and *in situ* birds, we calibrated the E-shaped tendon force buckles before *in situ* data collection by using the ergometer to induce sinusoidal length changes on the muscle while measuring length and force. We completed the calibration of the tendon buckle before starting the *F–L* and *F–V* experiments to allow the buckle to be removed for the *in situ* experiments. We calculated buckle calibration using a linear regression fit to the loading phase of the sinusoidal oscillations, to convert the measured strain voltage into a force in newtons. The buckle calibrations were found to be linear within the recorded range of forces (maximum 38±19 N, mean±s.d.), with a mean (±s.d.) R^2 of 0.95±0.06 and range between 0.85 and 0.99.

To induce muscle contractions, the sciatic nerve was stimulated using 0.2 ms square wave pulses at 100 Hz (4100 High Power Stimulator, A-M Systems, Carlsborg, WA, USA). We used twitch contractions at gradually increasing voltages to determine the optimal stimulation voltage (6.5–8.5 V). Stimulation trains with a 200 ms duration were used to construct the *F–L* relationship. Muscle force and muscle fascicle length were recorded at 1000 Hz using a National Instruments AD board (NI USB-6363) and Igor Pro 6.4 (Wavemetrics Inc., Lake Oswega, OR, USA). To construct the *F–L* curve, the LG was measured under isometric conditions at a series of lengths during fixed-end tetanic contractions (Fig. 1). For each individual, we used a 2nd degree polynomial fit to 9±1 individual contractions to obtain the *F–L* curve. This was determined based on the shape of the force maxima of a series of contractions: we aimed to obtain contractions that would capture the parabolic shape of the *F–L* curve. At each length, we first measured the passive force and length of the resting muscle, then the muscle was stimulated maximally for 200 ms (ensuring a near-maximum tetanic contraction), and the maximum active isometric force and corresponding fascicle length were measured for each contraction. We used 200 ms stimulation to minimize muscle fatigue. From the series of *F–L* experiments, we determined the maximum tetanic force (F_{max}), as well as the optimal fascicle length at which this F_{max} is produced (L_0). F_{max} was confirmed during a 400 ms contraction and was found to deviate minimally (±4% s.d.) from that measured for 200 ms stimulation.

The *F–V* relationship was determined through a series of 8–10, 400 ms after-loaded isotonic contractions. Force was allowed to rise to a predefined level between 0.1 and 0.9 of F_{max} and then the muscle was allowed to shorten while maintaining constant force. Forces and corresponding velocities were measured during a 30 ms period after the force had reached a stable plateau (Fig. 2).

Journal of Experimental Biology (2024) 227, jeb246879. doi:10.1242/jeb.246879

In situ data analysis

We fitted a second-degree polynomial curve (polynomial curve fitting tool, MATLAB 2022a, MathWorks) to the active and passive F–L curve. Based on these curves we determined the peak isometric force (F_{max}) and optimum length (L_0) from the fitted active F–L curve. To ascertain the activation dependence of L_0 (i.e. Holt and Azizi, 2014), in one individual we measured the F–L relationship for twitch and brief 50 ms tetanic contractions, resulting in submaximal forces between a twitch and maximally tetanic contraction. We determined the corresponding peak isometric force and optimum length under these submaximal conditions. Data were then normalized to F_{max} and L_0 (after Holt and Azizi, 2016).

We fitted a standard hyperbolic equation in MATLAB to determine the F–V curve, and normalized velocity to L_0 per second ($L_0\ s^{-1}$) to allow comparison of the F–V relationship among birds. We

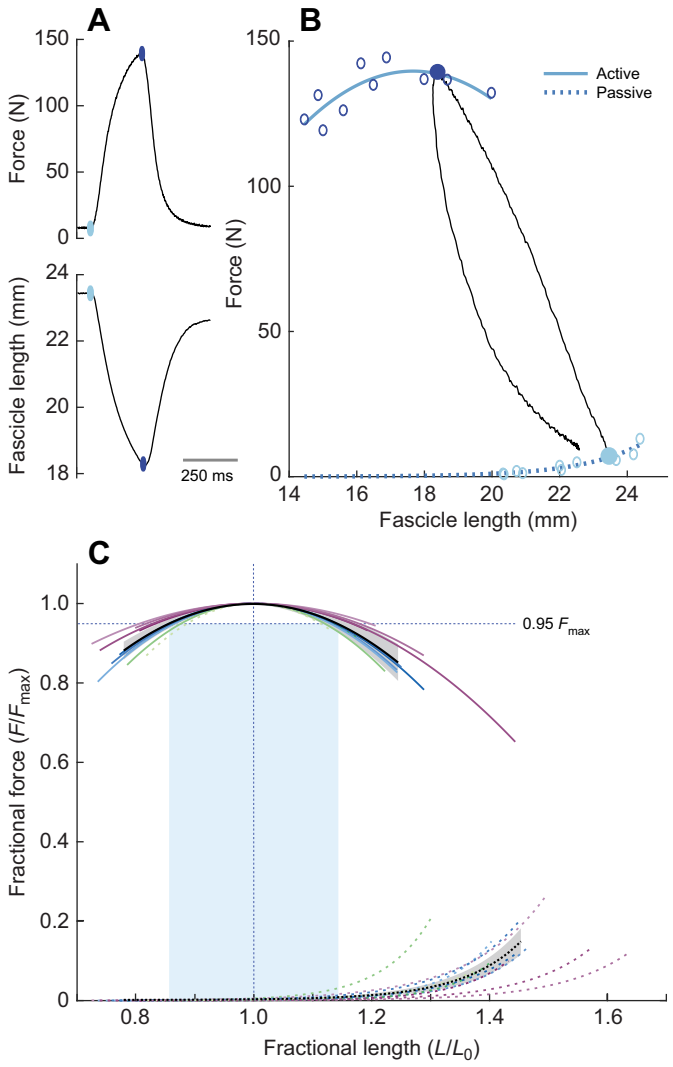

Fig. 1. Measuring the force–length relationship. The force–length (F–L) relationship was determined through a series of 200 ms tetanic contractions at varying fixed-end isometric lengths (see Materials and Methods). For each contraction (example in A), we measured the passive force and corresponding fascicle length (light blue) and the fractional length and total force during activation (dark blue). The active force was calculated by subtracting passive force from the total force. (B) After a series of contractions, we fitted separate curves to the active and passive F–L data (solid and dashed lines, respectively). For illustration, the individual contraction cycle from A is overlaid onto the corresponding F–L curve in B. (C) We normalized data to force as a fraction of maximum tetanic force (F_{max}), and length divided by the optimal length (L_0) to calculate fractional length. Different colored lines correspond to different individuals; active and passive force are shown by solid and dashed lines, respectively. The group average and 95% confidence interval (CI) are shown by the black line and shading. The shaded vertical rectangle indicates the strain width of the force plateau, defined using a force threshold of 0.95 F_{max} (indicated by the horizontal dashed line).

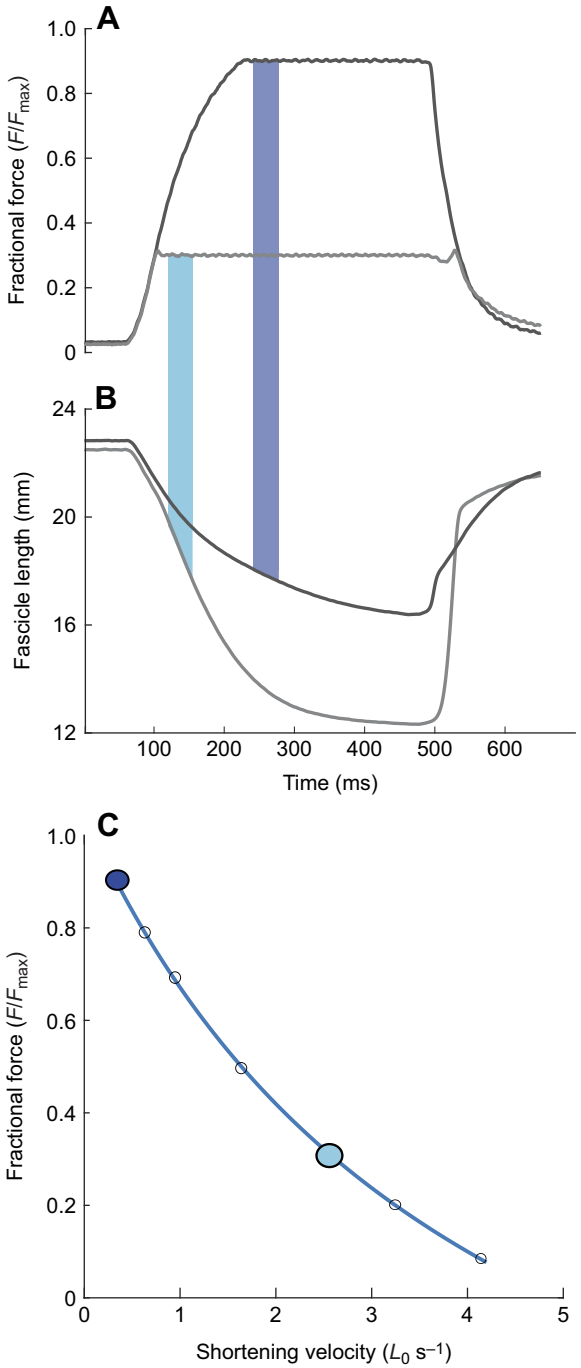

Fig. 2. Measuring the force–velocity relationship. (A,B) The force–velocity relationship (F–V) was obtained from a series of isotonic contractions at varying levels of fractional force. Two examples are shown here, for 0.3 F_{max} (light blue) and 0.9 F_{max} (dark blue) contractions. (C) The F–V relationship was fitted to data from each individual bird, using a hyperbolic curve fitting (representative example).

Journal of Experimental Biology (2024) 227, jeb246879. doi:10.1242/jeb.246879

multiplied force by velocity from the fitted F–V curve to obtain the power curve. From the power curve, we determined the peak power and the optimal shortening velocity at which peak power is produced, V_{opt}.

Morphological measures and normalization of *in vivo* and *in situ* data

We obtained muscle fascicle lengths ($L_{fascicle}$), muscle length and thickness using calipers while the muscle was under passive tension that corresponds to an active muscle fascicle length of L_0. All measured morphological parameters are presented in Table S1. These measurements were used to calculate the fractional length correction factor ($L_{fascicle}/L_{crystals}$) used to convert sonomicrometry distance to the total fascicle length, assuming homogeneous strain. This assumption is unlikely to lead to substantial errors because the LG fascicles are relatively short and $L_{crystals}$ was large relative to $L_{fascicle}$. Crystal alignment relative to the fascicle axis was verified post-mortem, and found to be within ±13 deg, indicating that errors due to crystal misalignment were <3%. The fractional length correction factor was also applied to *in vivo* data to calculate total fascicle length and strain. We calculated the physiological cross-sectional area (PCSA) from the animal's LG and combined LG and MG (total gastrocnemius) muscle mass divided by muscle density multiplied by fascicle length (L_0) (Alexander and Vernon, 1975).

After obtaining the F–L and F–V curve for each bird, we normalized muscle fascicle length, velocity and muscle–tendon force to the optima based on the contractile parameters obtained for that individual. Specifically, we normalized fascicle length by dividing instantaneous length by L_0. We calculated velocity normalized to optimal fascicle length, in units of L_0 s^{-1}. The LG maximum isometric stress was calculated by dividing LG maximum isometric force (F_{max}) by LG PCSA. *In vivo* stress was calculated by dividing *in vivo* measured gastrocnemius force by the combined gastrocnemius (LG and MG) PCSA, based on the simplifying assumption of uniform stress and strain between LG and MG. An estimate of total gastrocnemius F_{max} was calculated based on the assumption of uniform stress between LG and MG, resulting in force contributions proportional to PCSA. The total gastrocnemius PCSA was calculated to be 2.45× LG PCSA; therefore, total gastrocnemius F_{max} was calculated by multiplying LG F_{max} by 2.45. *In vivo* fractional force was then calculated by dividing instantaneous *in vivo* force by total gastrocnemius F_{max} (Table S1). To estimate the stiffness of the combined tendon and aponeurosis, we measured the fascicle shortening during a maximal tetanic fixed-end contraction, which is approximately equal to tendon stretch in these conditions, and then divided by the measured maximum force.

Statistical analysis

Summary values in the text are provided as means±s.d., unless otherwise specified. To test the main hypotheses of our study, we compared fascicle lengths and velocity at specific time points in the *in vivo* stride cycle with the *in situ* measured values of L_0 and V_{opt}. We used a paired t-test (ttest, MATLAB 2021a, MathWorks) to test the following: (1) whether muscle fascicle length at the time of peak force (F_{pk}) differed significantly from L_0, (2) whether muscle fascicle shortening velocity at T_c differed significantly from V_{opt}, and (3) whether muscle fascicle shortening velocity at F_{pk} differed significantly from 0. Paired t-tests are appropriate for the analysis because all statistical comparisons were made between the *in vivo* and *in situ* values measured within the same muscle and individual bird. To characterize the *in vivo* operating range, we measured *in vivo* lengths and velocities for time points spanning the active period: T_{act}, T_c, T_{rise}, T_{peak}, T_{fall} (defined above in '*In vivo* data analysis'), and calculated the mean and standard deviation across individuals.

To characterize potential dynamic strain effects observed *in vivo* during walking and running, we used linear mixed-effects (LME) models (fitlme, MATLAB 2021a, MathWorks) to test for relationships between strain and force and specific time points. In the first LME analysis, we tested the relationship between the *in vivo* observed passive force and corresponding muscle fascicle strain and velocity during passive force rise. In this statistical analysis, the peak magnitude of the *in vivo* passive force during early swing was the response variable (Y). We investigated fascicle strain, fascicle velocity and gait (walk, run) as predictors, with individual as a random effect. We compared multiple models. Model 1 included only the intercept and individual as a random effect: [Y∼1 + (1|individual)]; we used this as a reference model and null hypothesis. This reference model was compared to five alternative models: Model 2: [Y∼1 + strain + (1|individual)]; Model 3: [Y∼1 + velocity + (1|individual)]; Model 4: [Y∼1 + gait + (1|individual)]; Model 5: [Y∼1 + strain * velocity + (1|individual)]; and Model 6: [Y∼1 + gait + strain * velocity + (1|individual)]. We compared candidate models based on their Akaike's information criterion (AIC), total adjusted R^2, and log-likelihood ratio tests, which supported the selection of Model 6 across all variables tested.

In a second LME analysis on the *in vivo* data, we used a linear mixed-effects ANOVA to test whether the magnitude of the late-swing *in vivo* passive force was a significant predictor of total active force during stance. In this test, the maximum *in vivo* active force during stance was a response variable (Z). We compared two models. Model 1 included only the intercept and individual as a random effect [Z∼1 + (1|individual)'], which we used as a reference model and null hypothesis. This reference model was compared with the alternative model in which the peak late-swing passive force is a continuous linear predictor [Z∼1 + passive force magnitude + (1|individual)]. Based on a similar selection to that described above, Model 2 was statistically supported.

RESULTS

For each guinea fowl, a series of isometric contractions was used to construct the passive and active curves of the LG F–L relationship (Fig. 1A,B). Across all birds (n=11), the maximum LG force measured was 136±24 N. Stress was calculated by dividing peak force (F_{max}) by PCSA (Table S1), resulting in measures of maximum muscle stress with a mean of 278.9±47.2 kPa (Table 1). To compare the shape of the active and passive F–L curves across birds, we normalized the force to the maximum force (LG F_{max}) and the fascicle length to L_0 (L/L_0) (Fig. 1C), using the morphological measures (Table S1). The polynomial fit to the FL

Table 1. Summary of key measurements from the LG *in situ* force–length (*F–L*) and force–velocity (*F–V*) relationships across individuals

	Mean±s.d.
L_0 (mm)	19.7±1.4
F_{max} (N)	135.97±24.38
Peak stress (kPa)	287.9±47.2
V_{opt} (L_0 s^{-1})	2.9±0.4
P_{max} (W kg^{-1} muscle)	316.4±92.0

For each measurement we present the mean±1 s.d. across n=11 individuals. Peak stress was determined based on peak isometric force under maximally activated conditions, divided by physiological cross-sectional area calculated based on muscle mass and fascicle length (see Table S1). L_0, optimal length; F_{max}, peak force; V_{opt}, optimal velocity; P_{max}, maximum power.

Journal of Experimental Biology (2024) 227, jeb246879. doi:10.1242/jeb.246879

data had an average R^2 of 0.83±0.095 (Table S3). In comparing the results between the 'combined' and '*in situ* only' cohorts, the maximum forces averaged 136.0±24 N for combined and 133.7 ±16 N for *in situ* only, with no significant difference between the groups (P=0.8). Across all birds, we found that active isometric force remained within 0.95 F_{max} over a large range of fractional fascicle lengths (0.29±0.05 L_0) (Table S2). The force plateau started at an average length of 0.85±0.02 L_0, and ended at an average length of 1.13±0.04 L_0. Passive forces remained low across the active *F–L* curve, but showed high variation among individuals at long fractional lengths (Fig. 1C). Although we do not have an explanation for this variation, the passive forces consistently occurred at long lengths relative to L_0 and, consequently, the variation does not substantially impact force predictions over the observed *in vivo* operating ranges. We found only weak correlations between the free tendon length in the *in situ* preparation (i.e. the length between the muscle–tendon junction and the tendon clamp) and the *F–L* plateau width, V_{opt}, F_{max} and total fixed end compliance measured across birds (R^2 of 0.01–0.13; Table S2). This may reflect that a large fraction of the tendon compliance occurs in the aponeurosis rather than the free tendon, and suggests that the variation in free tendon length was not the main source of individual variation in our dataset.

The LG *F–V* relationship for each individual was constructed based on a series of individual isotonic contractions at different levels of fractional force (Fig. 3). As an example, we show measurements from two trials from an individual bird, with force set at 0.3 and 0.9 F_{max} (Fig. 2A,B), and illustrate where these individual measurements fall on the resulting *F–V* curve (Fig. 2C). We multiplied force by velocity from the fitted *F–V* curve to obtain the power curve and the optimal shortening velocity at peak power output (V_{opt}). The mean normalized V_{opt} across all birds occurred at 2.9±0.4 L_0 s^{-1} (Fig. 3). The mean force at V_{opt} was 0.41±0.04 F_{max}. Summary values from the *F–L* and *F–V* experiments are provided in Table 1. The average R^2 of the *F–V* curve was 0.985±0.02. Detailed fit parameters and goodness of fit results of the *F–L* and *F–V* curves can be found in Table S3.

In vivo muscle force, fascicle length and activation were used to construct muscle work loops for walking and running. A representative sequence of four strides shows typical force, length and activation patterns over time (Fig. 4). Work loop shape was relatively repeatable across strides in steady walking and running, but varied among individuals, as shown for two representative individuals in Fig. 5. These examples represent the range of variation in work loop shape across individuals in the current dataset. Some individuals exhibited near-isometric contraction, with a narrow force peak (Fig. 5A,B) and others exhibited substantial shortening throughout force development, resulting in an open work loop shape and higher work output (Fig. 5C,D). In running, total work output was higher as a result of a combination of higher peak force and greater shortening during force development compared with walking (Fig. 5).

To test the hypothesis that muscle fascicle length at time of peak force (F_{pk}) differed significantly from L_0, we compared *in vivo* values of length at F_{pk} for walking and running with L_0 (Fig. 6). At F_{pk} in running, fascicle length was 0.77±0.12 L_0, which is significantly shorter than L_0 (P=0.002). Similarly, during walking, F_{pk} occurred at 0.77±0.13 L_0, which is significantly shorter than L_0 (P=0.002). These data indicate that *in vivo* force production during walking and running mainly occurs on the ascending limb of the maximal tetanic *F–L* curve. We also compared the *in vivo* operating lengths to the *F–L* curve at lower activation levels that correspond more closely to submaximal *in vivo* activation (Fig. 6B). Lower activation levels resulted in a rightward shift of the *F–L* curve

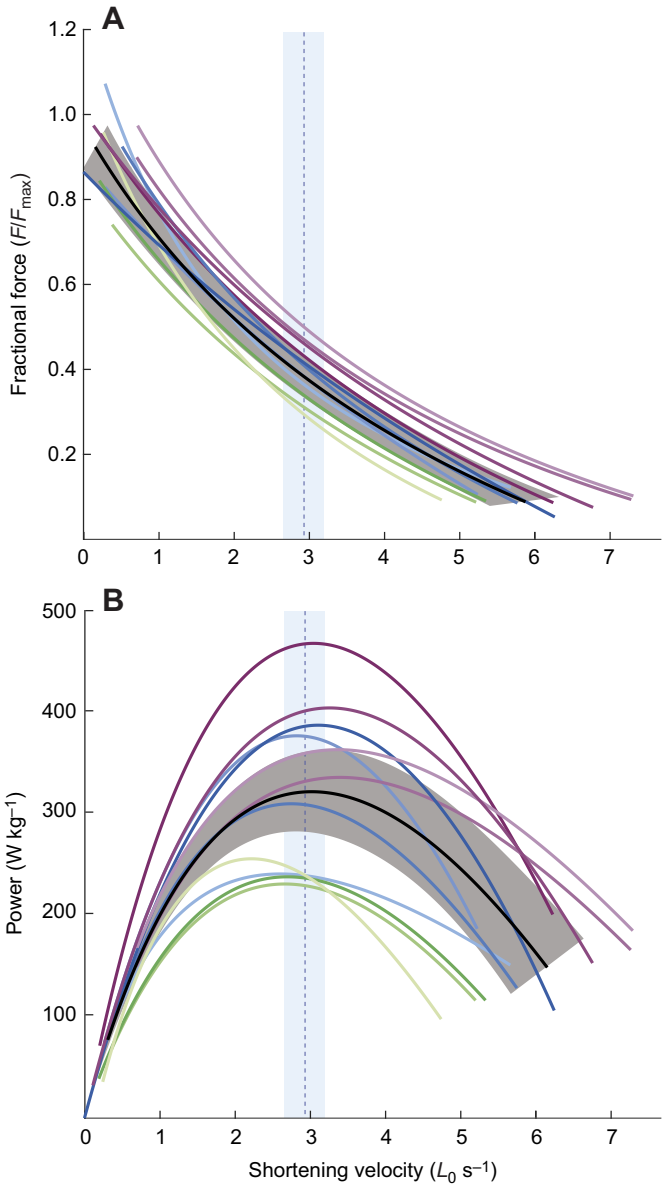

Fig. 3. *F–V* relationships across individuals. (A) The *F–V* relationships across individuals (n=11) in normalized units. (B) Power curves are shown in watts per kilogram muscle. Each color indicates a different individual. The vertical dashed line and blue shading indicate the mean optimal velocity (V_{opt}; 2.9 L_0 s^{-1}) and the 95% confidence interval (CI). Black lines and gray shading indicate the group average and 95% CI of the *F–V* and power curve across birds.

(towards longer lengths), which puts *in vivo* operating ranges even further down the ascending limb of the submaximal *F–L* curve (Fig. 6B).

To test the hypothesis that the LG fascicles shorten at V_{opt} while producing power during walking and running, we compared *in vivo* shortening velocities with V_{opt} at the time of foot contact (T_c) when force is low and power is near its *in vivo* peak (Fig. 7). In walking, at T_c, shortening velocity averaged 2.33±1.5 L_0 s^{-1}, and did not differ significantly from V_{opt} based on a paired *t*-test (P=0.36). In running, velocity at T_c averaged 2.69±1.1 L_0 s^{-1} and did not differ significantly from V_{opt} based on a paired *t*-test (P=0.54). The *in vivo* operating values are shown graphically relative to the *F–V* curve in Fig. 7.

Journal of Experimental Biology (2024) 227, jeb246879. doi:10.1242/jeb.246879

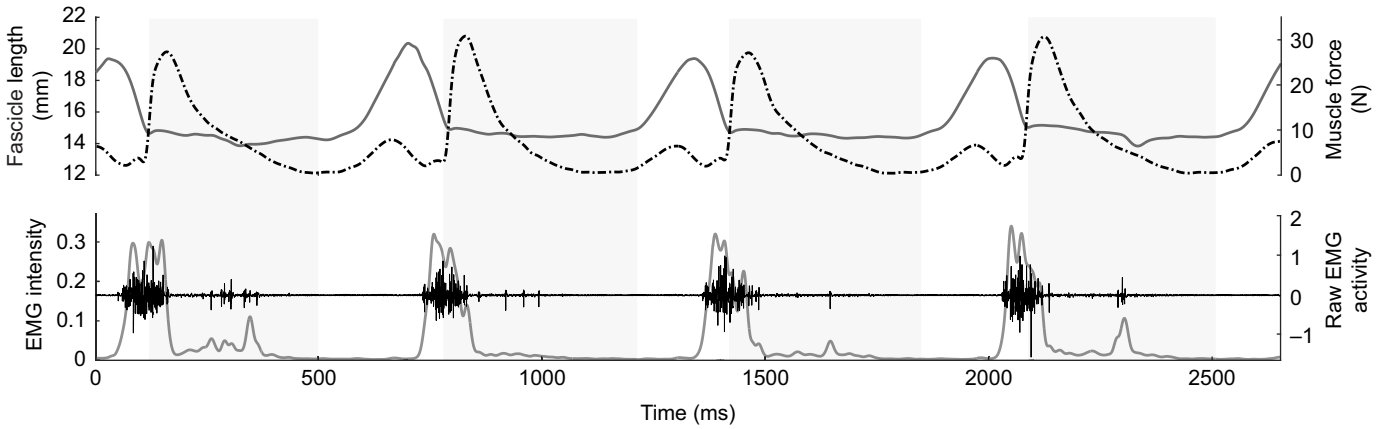

Fig. 4. Representative *in vivo* data recording. Muscle fascicle length (top, left *y*-axis, solid line), muscle force (top, right *y*-axis, dashed line), EMG intensity (see Materials and Methods; bottom, left *y*-axis) and raw EMG signals (bottom, right *y*-axis) for four consecutive strides for a single bird during walking. Gray shaded blocks indicate times of foot–ground contact.

To test the hypothesis that LG operates near zero velocity (isometric contraction) while producing high forces during walking and running, we statistically compared the *in vivo* values of velocity at peak force during stance (F_{pk}) to zero velocity (Fig. 7). Muscle fascicle shortening velocity was lower at F_{pk} compared with T_c in both walking and running. At F_{pk}, velocity averaged 0.02 ±0.33L_0 s^{-1} in walking which did not differ significantly from zero (P=0.89). Similarly, in running, velocity at F_{pk} averaged 0.03±0.3 L_0 s^{-1} which did not differ significantly from zero (P=0.91).

In vivo operating ranges in walking and running

We also characterized *in vivo* operating ranges throughout the period of muscle activity during walking and running (Fig. 6A). The differences in active muscle operating ranges between walking and running were minimal. The active fractional length range of 0.73–1.11 L_0 in running was only slightly wider that of walking (0.76–1.07 L_0). *In vivo* peak muscle forces were 16% higher in running versus walking, and both were far below the maximally tetanic F_{max}. Walking F_{pk} measured 0.09±0.02 F_{max}, while running F_{pk} measured 0.13±0.03 F_{max}, based on dividing *in vivo* F_{pk} by total gastrocnemius F_{max} (see Materials and Methods). In both gaits, muscles were activated at lengths close to the isometric *F–L* plateau. In walking, length at T_{act} did not differ significantly from L_0 (P=0.09), whereas in running, length at T_{act} was slightly longer than L_0 (P=0.01) (Table 2). Activation was followed by rapid shortening across the *F–L* plateau at low forces. However, significant force rise did not occur till after T_c. At T_c in walking, fascicle length averaged 0.79±0.14 L_0, significantly shorter than L_0 (P=0.002). Shortly after T_c, a sharp rise in force occurred (measured as F_{rise}) leading to peak force (F_{pk}). In running, fascicle length at T_c averaged 0.77±0.1 L_0, significantly shorter than L_0 (P=0.002). Despite slightly higher forces in running, shortening velocity was similar between gaits. Lastly, we tested for a correlation between muscle–tendon stiffness and work loop shape. We found a trend toward higher measures of *in vivo* net work with lower *in situ* muscle–tendon unit (MTU) stiffness (i.e. higher compliance), indicating more open work loops (walking R^2=0.13, and running R^2=0.29). While the correlation was stronger for running, it was not statistically significant for either gait because of the low sample size (n=6 for *in vivo* data).

Muscles exhibited a passive force rise during late swing during both gaits, indicated by an increase in force in the absence of EMG activity (Figs 4 and 5). This passive force rise occurred during rapid passive stretch (Figs 4 and 5), but at fascicle lengths near 1.0 L_0 where no significant passive force was observed for the *in situ* passive *F–L* curve (Fig. 1). The peak magnitude of the late-swing passive force correlated with passive muscle fascicle strain, strain rate and their interaction (strain: F stat=40.6, P<0.001, strain rate: F-stat=197.9, P<0.001, strain×strain rate: F-stat=352.7, P<0.001). Gait also had a significant effect on the peak passive force (gait: F-stat=85.9, P<0.001), indicating that passive force was significantly higher during running than during walking. The magnitude of the passive force during swing was also a significant positive predictor of the magnitude of the active force during the subsequent stance (F-stat=125.3, P<0.001).

Table 2. Summary of *in vivo* length (L_0) and velocity (L_0 s^{-1}), normalized to *in situ* optimum length (L_0)

		Length (L_0)	Velocity (L_0 s^{-1})
Walk	T_{act}	1.05±0.06	1.27±0.28
	T_c	0.79±0.09	2.33±1.47
	T_{rise}	0.77±0.08	1.21±1.31
	T_{pk}	0.76±0.09	0.02±0.33
	T_{fall}	0.73±0.09	0.48±0.36
Run	T_{act}	1.09±0.05	0.58±2.04
	T_c	0.78±0.09	2.89±1.09
	T_{rise}	0.77±0.07	1.30±1.51
	T_{pk}	0.77±0.09	0.03±0.3
	T_{fall}	0.71±0.09	1.76±0.91

Mean±1 s.d. measures of fractional fascicle length and velocity at specific time points in the active period: time of onset of muscle activation (T_{act}), time of foot contact (T_c), time of force rise (T_{rise}), time of peak force (T_{pk}) and time of force fall (T_{fall}). Measures are presented for walking (top) and running (bottom).

DISCUSSION

In the current study, we compared dynamic, *in vivo* operating ranges of the LG of guinea fowl with the measured *in situ* isometric *F–L* and isotonic *F–V* relationships. Muscle physiological properties characterized using the *F–L* and *F–V* relationships have been used to predict and interpret dynamic *in vivo* muscle dynamics (i.e. Rome, 1998; Burkholder and Lieber, 2001; Lieber and Ward, 2011). Based on previous work, we hypothesized that muscles operate near optimal conditions for force during mid stance, and for power production during the swing–stance transition during walking and running. Our findings partially support the hypothesis that muscle fascicles operate near optimal conditions during walking and running – consistent with the isotonic *F–V* relationship, we found that the LG operated at low

Journal of Experimental Biology (2024) 227, jeb246879. doi:10.1242/jeb.246879

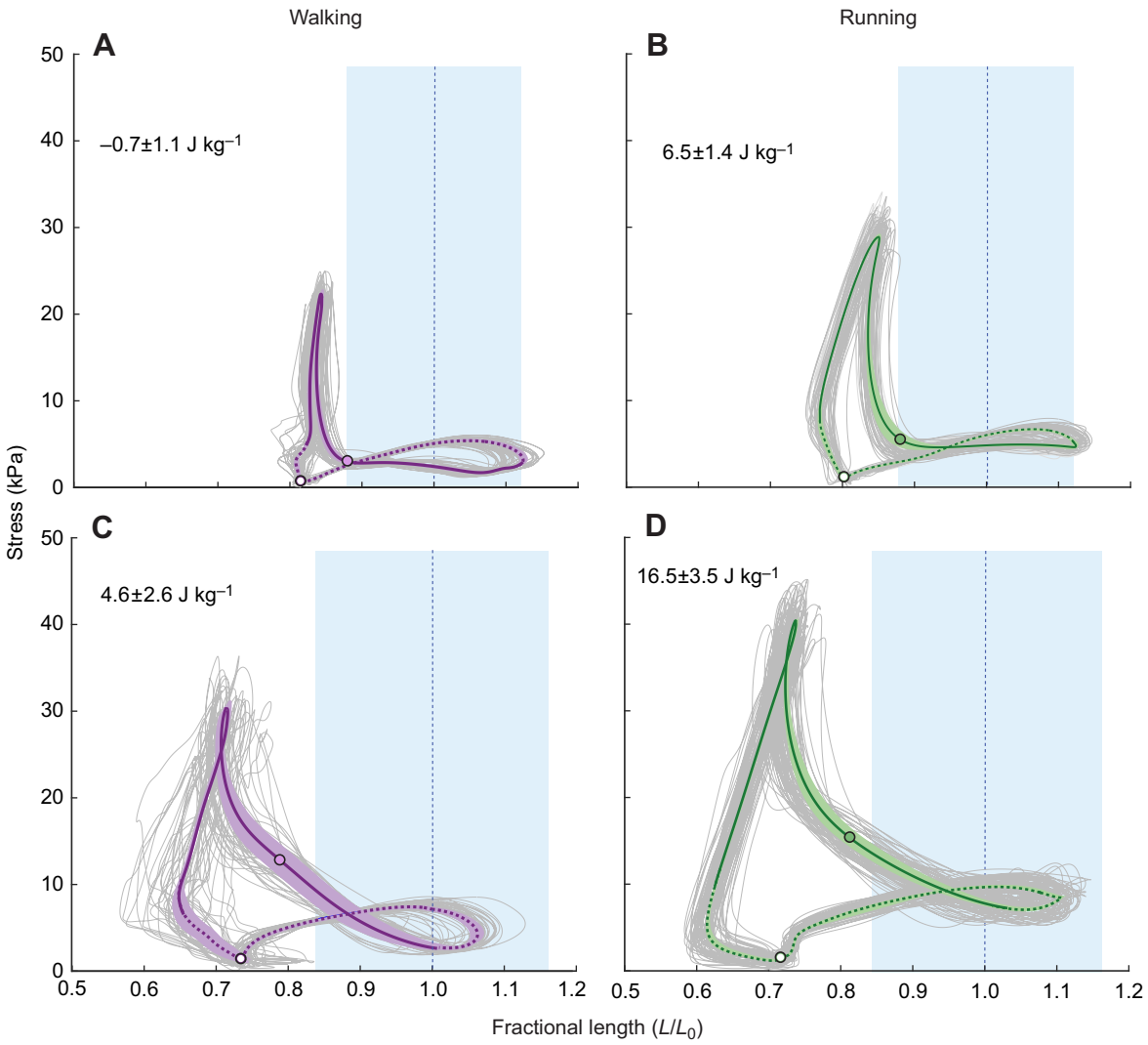

Fig. 5. Representative work loops during walking (left) and running (right) of two representative individuals (ind2 and ind7). All work loops of the trial are plotted in gray. Averages are represented by the colored lines; shaded areas around the lines indicate the 95% CI. The time of EMG activity is represented by the solid lines, and dashed lines indicate no EMG activity. Filled circles indicate the time of foot contact (T_c) and open circles indicate the time of foot take-off (T_{off}). The strain width of the same individual's *F–L* force plateau is indicated by the blue shaded rectangle. The represented individuals were selected to span the observed range of *in vivo* lateral gastrocnemius (LG) function, the most (A,B) and least (C,D) isometric during stance LG in walking and running. The mass-specific work output is indicated in each panel (means±s.d.).

velocity at peak force, but at velocity near V_{opt} at the swing–stance transition, when the guinea fowl LG produces positive work in walking and running. Our findings are consistent with a previous study on turkey gastrocnemius and plantaris muscle, where investigators found low average shortening velocity (<0.1 V_{max}) at peak force (Gabaldón et al., 2008). Although not directly reported, data from Gabaldón et al. (2008) suggest that shortening velocity is also considerably higher at T_c compared with peak force (see fig. 6 in Gabaldón et al., 2008). These findings are consistent with *in vivo* optimization for economy of forces at higher loads and power during work production, as previously suggested for the turkey gastrocnemius (Roberts et al., 1997). However, we also found that the guinea fowl LG shortens rapidly at low forces across the *F–L* plateau and produces the highest *in vivo* forces at lengths around 0.8 L_0. This indicates that the LG mainly develops force at lengths below the optimal length predicted based on the *F–L* plateau. We also observed that the *F–L* curve shifts rightward (to longer lengths) with submaximal activation; therefore, the *in vivo* operating ranges correspond to lengths further down the ascending limb of the submaximal *F–L* curve (Fig. 6B).

Distal ankle extensor muscles such as the LG have a bi-articular architecture with pennate fascicles and long in-series tendons that decouple muscle fascicle and MTU dynamics (Roberts et al., 1997; Azizi and Roberts, 2014; Schwaner et al., 2021). Previous work suggests that the bi-articular LG MTU acts to control energy transfer across joints and provide ankle propulsion (i.e. Gregoire et al., 1984; Zajac et al., 2002; Lichtwark and Wilson, 2006; Schwaner et al., 2018). Under the conditions studied here, we found that guinea fowl LG work loops exhibit an L-shape (Fig. 3A), which suggests a mostly strut-like function of the muscle fascicles during stance, similar to the turkey LG (Roberts et al., 1997). At the swing–stance transition, LG muscle fascicle shortening work occurs simultaneously with energy absorption at the ankle joint (Daley and Biewener, 2003; Daley and Biewener, 2007; Daley et al., 2009), suggesting that muscle fascicles shorten against the tendon while the tendon stretches under load. For reference, individual example

Journal of Experimental Biology (2024) 227, jeb246879. doi:10.1242/jeb.246879

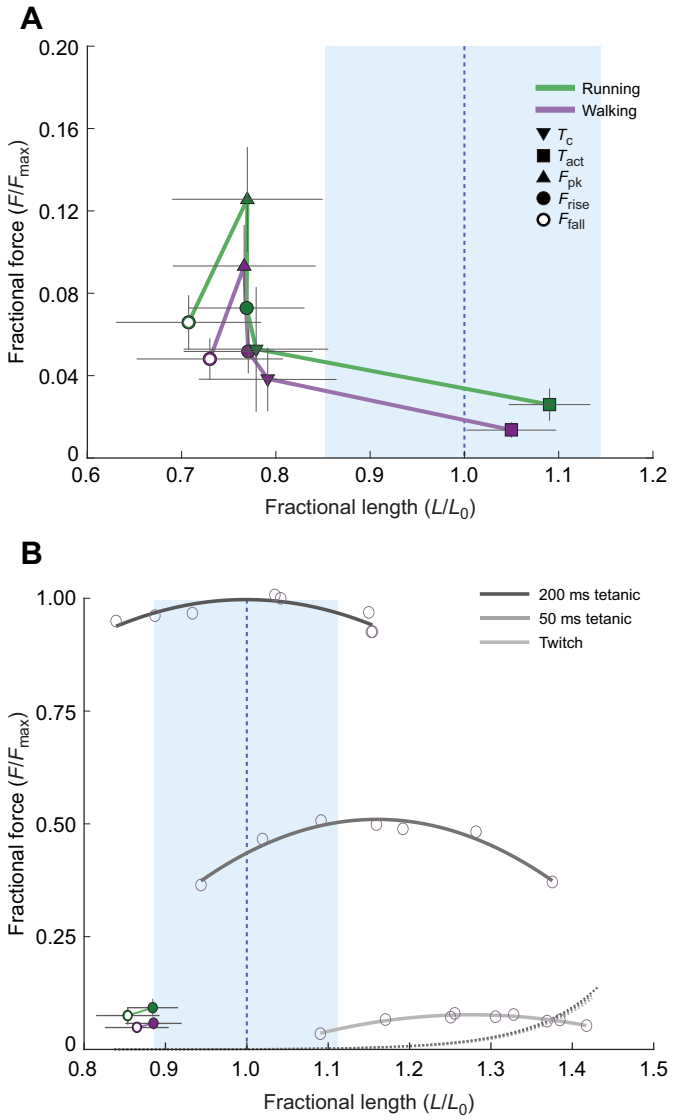

Fig. 6. *In vivo* muscle–tendon force and fascicle strain operating ranges relative to the *F–L* plateau. (A) To summarize *in vivo* data across individuals, we show fractional force and length at the time of onset of muscle activation (T_{act}), T_c, force rise (F_{rise}), peak force (F_{pk}) and force fall (F_{fall}). Error bars indicate 95% CI. The blue shaded rectangle indicates the strain width of the *F–L* force plateau. The muscle is activated at lengths slightly longer than the L_0, and rapidly shortens at low force across the plateau. Little force rise occurs until foot contact (T_c), and F_{pk} occurs during stance at fractional lengths near 0.8 L_0. (B) The effect of activation on the *F–L* relationship for a single representative individual. Active *F–L* relationships with tetanic 200 ms stimulation (top), tetanic 50 ms stimulation (middle) and twitch stimulation (bottom). The blue shaded rectangle indicates the strain width of the individual's *F–L* force plateau. The corresponding passive curves (dashed) are shown but overlap. Open circles indicate individual data points from a single isometric contraction. For comparison, in A we show the *in vivo* force and fractional length at 50% force rise and decay for walking (purple) and running (green) of the same individual. With decreasing stimulation and isometric force magnitude, the *F–L* plateau shifts rightward to longer optimal muscle lengths compared with the maximum tetanic curve.

traces of muscle dynamics (e.g. length, activation, force) with corresponding knee and ankle angle trajectories for walking and running are provided in Figs S1 and S2. During early stance, the ankle joint absorbs energy; therefore, the positive LG work does not directly power joint work. It is interesting that the fascicles shorten near V_{opt} even when the muscle is not directly powering joint or limb propulsion. In late stance, positive power occurs at the ankle, yet muscle fascicles contract near isometrically, while elastic energy cycling occurs in the tendon, as observed in turkeys and wallabies (Roberts et al., 1997; Griffiths, 1989). These findings suggest that in steady gait, the guinea fowl LG mainly controls energy transfer across joints, rather than directly actuating the ankle joint. Considering that the LG mainly acts to regulate force and energy transfer during stance, it is perhaps surprising that the LG muscle fascicles do not operate on the *F–L* plateau for optimum economic force production. However, we note that the *F–L* curve suggests the active isometric force remains within 0.95 F_{max} of the maximum force over a large range of fractional fascicle lengths, with a strain width of 0.29±0.05 L_0. Additionally, *in vivo* walking and running forces are far below the tetanic F_{max}. Operating at shorter than optimal fractional lengths may not be ideal for force economy (Roberts et al., 1997); however, it is unlikely to limit force output because the *in vivo* forces in walking and running are so far below the tetanic F_{max}.

There may be a functional benefit to operating at lengths shorter than optimal in steady state. Obstacle perturbations sometimes require a sudden increase in muscle force development at longer fascicle lengths; for example, in uneven terrain (Daley and Biewener, 2011). Additionally, evidence shows pre-shortening of plantar flexors to function as shock absorbers (Roberts and Konow, 2013; Dick et al., 2021). In guinea fowl, the LG starts shortening near L_0 at the time of EMG onset, yet force production during the stance phase in steady gait occurs almost entirely on the ascending limb of the *F–L* curve (0.7–0.8 L_0). Operating at lengths on the descending limb of the *F–L* curve may be a strategy for avoiding the muscle damage that could arise from a rapid stretch due to an unexpected perturbation. Here, the system needs to balance what is likely a complex trade-off between economic force generation, the ability to develop force rapidly to resist a minor stretch (which increases with length), and avoidance of instabilities associated with long sarcomere lengths. Although this pattern may not be optimal for steady treadmill locomotion, the additional force potential may provide intrinsic mechanical stability in the presence of rapid unexpected perturbations. In the presence of obstacles, guinea fowl LG experiences earlier loading due to earlier foot contact, resulting in an earlier and rapid rise in force, reaching a higher peak force (Daley and Biewener, 2011; Gordon et al., 2020; Schwaner et al., 2023). The muscle fascicles continue to shorten throughout the perturbation; therefore, increased force is not directly related to fascicle stretch. However, force development occurs at longer lengths in obstacle steps. The current findings suggest some of the increase in force in obstacle steps arises from higher force potential when the fascicles operate at lengths on the *F–L* plateau (Fig. 8). A steady-state work loop trajectory that operates at shorter than optimal lengths provides the potential for a rapid, intrinsic increase in muscle force when the operating length of the muscle fascicles is increased by a sudden abbreviation of the swing phase, reacting more rapidly than possible through reflexive changes in activity (Loeb et al., 1999; Daley et al., 2009). Therefore, the shortening of the LG across the *F–L* plateau in late swing may provide a mechanical safety factor against unexpected perturbations that require rapid force development in response to varied timing of foot contact.

Shortening across the *F–L* plateau may occur in cyclical tasks that involve abrupt transitions in external loading with uncertain timing. Shortening across the *F–L* plateau is also observed in frog plantaris and semimembranosus in hopping, the rat medial gastrocnemius

Journal of Experimental Biology (2024) 227, jeb246879. doi:10.1242/jeb.246879

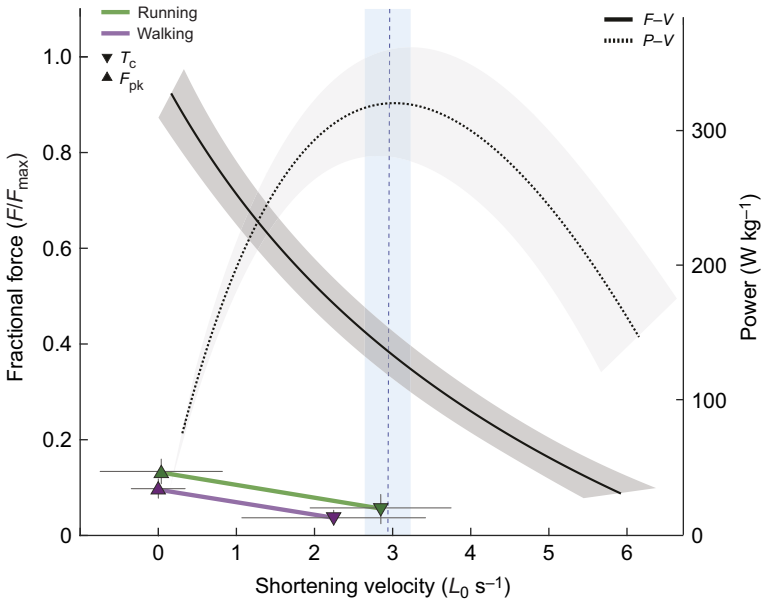

Fig. 7. Relating *in vivo* operating range to the *F–V* relationship. Mean velocity and normalized force at T_c and F_{pk} are shown along with the mean *F–V* (solid line) and power–velocity (*P–V*; dashed line) relationships across individuals. Shaded regions indicate 95% CI. The vertical dashed line indicates the average V_{opt} and the blue rectangle indicates the 95% CI for V_{opt}. Muscles shorten at low velocity at F_{pk}, and at higher velocity at T_c, when the muscle produces shortening work. Fractional forces are higher in running (green) compared with walking (purple).

during trotting, and the sternohyoid muscle during swallowing (Ahn et al., 2018; Holt and Azizi, 2016). In contrast, during jumping tasks, frog plantaris muscles primarily operate on the descending limb of the *F–L* curve (Azizi and Roberts, 2010). These patterns may relate both to the mechanical demands of the task and to the uncertainty in externally applied loads. Ballistic movements such as jumping may involve more predictable loading patterns compared with cyclical tasks that involve abrupt load transitions in contact with the external environment.

In examining variation among individuals, we note that variation occurred in the remaining free tendon length (length from muscle–tendon junction to clamp) in our *in situ* preparation, which contributed to variation in the measured stiffness in the fixed-end contractions. However, we found that the variation in free-tendon length explained only a small fraction of the observed variation among individuals in the outcome measures of the *F–L* and *F–V* experiments (see Table S2). This is likely because most of the compliance in the guinea fowl LG MTU arises from within the aponeurosis, not the free tendon. We did find a trend towards greater work output, with more open work loop shape, among individuals with higher measured MTU compliance (lower stiffness) (Table S3). This suggests that some of the observed individual variation in work loop shape during walking and running arises from individual variation in the LG MTU compliance. It would be useful to investigate this further in the future through more detailed analysis of the relationships between muscle–tendon morphology, tendon material properties and 3D shape change during dynamic contractions.

Despite more than a half a century of elegant and sophisticated experiments in isolated muscle physiology, our ability to establish a framework for predicting *in vivo* muscle performance remains remedial. One of the remaining and unresolved challenges in relating *in situ* and *in vivo* data is our inability to accurately and confidently replicate the activation dynamics driven by the nervous system.

This study along with numerous others focused on characterizing the *F–L* and *F–V* relationships used maximal stimulation of muscle in order to create comparable contraction conditions across different muscles. However, natural movements rarely require maximum activation of muscle, complicating integrative approaches to studying muscle function (Walmsley et al., 1978; Strojnik, 1995). The potential limitation of recreating *in vivo* recruitment patterns is not limited to standard approaches relying on isometric and/or isotonic contraction protocols. Despite significant advances in creating more realistic contractile conditions that better reflect *in vivo* function, most approaches still rely on near-maximal stimulation protocols (Robertson and Sawicki, 2015; Richards and Eberhard, 2020; Mendoza et al., 2023; Rice et al., 2023). Although our ability to recreate the complexity of *in vivo* motor unit recruitment is limited, previous studies have shown that shifts in the *F–L* and *F–V* relationship resulting from changes in activation level change the optimal length (L_0) and velocity (V_{opt}). A decrease in activation level has been shown to cause a rightward shift to longer lengths and lower forces in the *F–L* relationship (e.g. Holt and Azizi, 2014, 2016). We found a similar shift in the *F–L* curve with submaximal stimulation (Fig. 6B). Similarly, optimal velocity for power production has been shown to be at a relatively slower velocity at lower activation levels (Holt et al., 2014). As the complex relationship between activation and intrinsic muscle properties remains unresolved, results relating *in situ* and *in vivo* behaviors can become difficult to interpret. For example, *in vivo* data from walking, a clearly submaximal locomotor behavior, have been shown to map onto the ascending limb of the maximally determined *F–L* relationship (current study; Rubenson et al., 2012). As such, a rightward shift in the *F–L* curve would suggest that muscle fascicles are at too short a length to produce force. It is clear that our ability to work across levels of biological organization to develop an integrative understanding of muscle-powered movements is limited by the lack of a protocol to better recreate natural patterns of activation in reduced complexity preparations. Future studies aimed at developing an experimental framework for recreating a dynamic activation state in isolated muscles will greatly advance our current understanding of locomotor systems.

The isometric *F–L* and isotonic *F–V* relationships allow comparison of muscle contractile properties under standard and controlled conditions, but they do not capture non-linear interactions between strain trajectory and activation dynamics that influence force and work output during dynamic tasks (Askew and Marsh, 1998; Perreault et al., 2003; McGowan et al., 2013). We found that a passive force rise (i.e. in the absence of EMG activity) occurs in early swing (Figs 3 and 4) in walking and running. This passive force rise occurs at fascicle lengths that do not result in measurable muscle passive forces *in situ* (Figs 1 and 5). This

Journal of Experimental Biology (2024) 227, jeb246879. doi:10.1242/jeb.246879

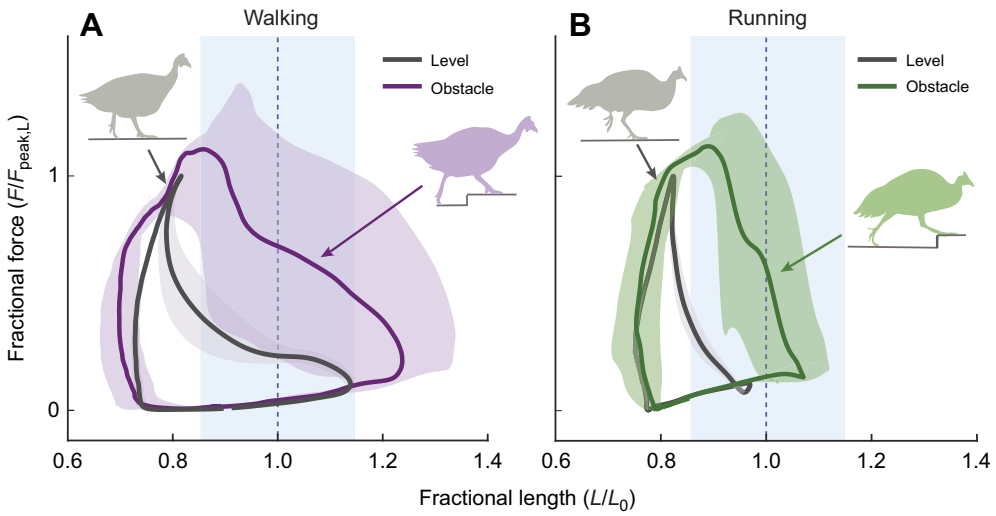

Fig. 8. LG work loops in obstacle strides compared with level strides in walking (left) and running (right). Data are from published studies on walking (A, Ind 3) and running (B, Ind 6) over obstacles (Gordon et al., 2020; Schwaner et al., 2023). Force was normalized relative to peak force during steady level gait ($F_{peak,L}$) at the same speed because F_{max} is unknown. Fascicle length was normalized such that peak force occurs at 0.8 L_0, as found in the present study. However, L_0 was not directly measured for these individuals. Shading around lines indicates 95% CI. The blue shaded rectangle indicates the average strain width of the force plateau across individuals from the current study. Obstacles elicit earlier and steeper force rises, at longer fractional lengths compared with level walking. Peak *in vivo* forces occur within the estimated *F–L* plateau in obstacle strides. This suggests that the low forces in late swing in steady strides create a safety buffer, with potential for the muscle to rapidly generate higher forces in response to unexpected perturbations, without a change in muscle activation.

suggests that the passive *F–L* relationship under static conditions cannot capture these observed forces, which might instead relate to dynamic viscoelastic properties or history-dependent effects, such as short-range stiffness, stretch-induced residual force enhancement, and passive force enhancement (Edman et al., 1982; Edman, 2012; Herzog, 2018; Seiberl et al., 2015; Hahn and Riedel, 2018). Viscoelastic properties and history-dependent effects can provide stability in response to perturbations as active control can tune intrinsic properties (Gregor et al., 1988; Loeb et al., 1999; Lappin et al., 2006). We found that the magnitude of the active force in the stance phase has a positive correlation with the magnitude of the passive force during swing, suggesting the importance of contributions of dynamic strain and strain rate histories to passive and active force development, even during steady-state *in vivo* conditions. Viscoelastic elements contribute to muscle force and work during steady-state locomotion, thereby assisting in stabilizing gait (Zajac et al., 2003; Hessel et al., 2021). However, we note that the Achilles tendon is the common tendon for the LG, MG and the intermediate gastrocnemius (IG) in guinea fowl, and therefore contributions from IG or MG, via either direct or lateral transmission of force, could contribute to the apparent passive forces. Yet, no significant MG EMG activity is observed in late swing during walking and running in guinea fowl (Gordon et al., 2015), and therefore we believe agonist contributions are unlikely to explain the observed passive force.

Given our findings here, it is critical that the approaches to studying isolated muscles advance beyond the standard historical protocols. While direct measures of muscle force and length *in vivo* may not be practical for all systems, recent technical advances provide the potential to bridge the gaps in current understanding by using real-time feedback control to allow isolated muscles to interact dynamically with models (physical or virtual) (Robertson and Sawicki, 2015; Richards and Eberhard, 2020; Mendoza et al., 2023). Further work is needed to develop new standardized protocols to characterize muscle under dynamic but controlled conditions, including work loops with sudden perturbations in force, activation or strain trajectory (Sponberg et al., 2023). Dynamic characterization of muscle contractile function is essential for understanding how the non-linear interactions between activation and strain trajectory influence muscle force and work output during realistic locomotor conditions.

This study provides a novel comparison of *in vivo* muscle operating forces, fascicle lengths and velocities with optimum *in situ* characterized lengths and velocities. We show that the guinea fowl LG muscle fascicles shorten near optimal velocities during force development *in vivo*, but do not operate on the *F–L* plateau during force development in walking and running. We also found a rise in passive force in the LG during early swing at fascicle lengths that correspond to negligible passive forces *in situ*. This finding suggests that *in vivo F–L* dynamics are substantially influenced by dynamic strain effects such as viscoelasticity, short-range stiffness and other lengthening force enhancement. Our study provides new evidence that the static nature of the *F–L* properties makes intrinsic muscle properties less predictive of *in vivo* behavior than previously thought. Direct comparison of *F–L* and *F–V* properties with *in vivo* muscle *F–L* dynamics and operating ranges also suggests the need to further examine how dynamic interactions between strain and activation influence muscle force and work output *in vivo*. Complex interactions between strain and activation are especially important during unsteady locomotor tasks, where muscle–tendon force and work output may be influenced by viscoelastic and other history-dependent aspects that are not captured in isometric *F–L* and isotonic *F–V* experiments.

Acknowledgements

The authors would like to acknowledge Elizabeth Mendoza for expert advice during *in situ* data collection. The authors would like to thank Adrien Arias, Vivian Chong, Brooke Christensen, Catalina Dentzel, Kamila Karimjee, Zhiji Li, Elizabeth Mendoza and Daisey Vega for help with *in vivo* data collection, and Chris Wagner for helping with the *in vivo* experimental set-up. We thank the UCI University Animal Laboratory Resources team for animal husbandry and veterinary care.

Competing interests
The authors declare no competing or financial interests.

Author contributions
Conceptualization: M.J.S., D.L.M., E.A., M.A.D.; Methodology: M.J.S., D.L.M., E.A., M.A.D.; Software: M.A.D., E.A.; Validation: M.J.S., D.L.M., E.A., M.A.D.; Formal analysis: M.J.S.; Investigation: M.J.S., D.L.M.; Resources: E.A., M.A.D.; Data curation: M.J.S., M.A.D.; Writing - original draft: M.J.S.; Writing - review & editing: M.J.S., D.L.M., E.A., M.A.D.; Visualization: M.J.S.; Supervision: E.A., M.A.D.; Project administration: M.A.D.; Funding acquisition: E.A., M.A.D.

Funding
This work is funded by a postdoctoral PDM-II fellowship from KU Leuven (to M.J.S.), the National Science Foundation (NSF) (grant 2016049 and 2319710 to M.A.D.) and the National Institutes of Health (NIH) (grant R01 AR055295-09 to E.A.). Deposited in PMC for release after 12 months.

Data availability
The data underlying this research article, including MATLAB files containing continuous *in vivo* recordings of muscle length, force and activation of running and walking guinea fowl, and the measured characteristics from the *in situ F–L* and *F–V* experiments, plus an Excel file of the data underlying our statistical tests, are available from the Dryad digital repository (Schwaner et al., 2024): https://doi.org/10.5061/dryad.0p2ngf26p

References

Ahn, A. N. (2012). How muscle function – the work loop technique. *J. Exp. Biol.* **215**, 1051-1052. doi:10.1242/jeb.062752
Ahn, A. N., Konow, N., Tijs, C. and Biewener, A. A. (2018). Different segments within vertebrate muscles can operate on different regions of their force–length relationships. *Integr. Comp. Biol.* **58**, 219-231. doi:10.1093/icb/icy040
Alcazar, J., Csapo, R., Ara, I. and Alegre, L. M. (2019). On the shape of the force-velocity relationship in skeletal muscle: the linear, the hyperbolic, and the double-hyperbolic. *Front. Physiol.* **10**, 00769. doi:10.3389/fphys.2019.00769
Alexander, R. M. and Vernon, A. (1975). The mechanics of hopping by kangaroos (Macropodidae). *J. Zool.* **177**, 265-303. doi:10.1111/j.1469-7998.1975.tb05983.x
Always, S. E. (1995). Slowing of contractile properties in quail skeletal muscle with aging. *J. Gerontol. A* **50A**, B26-B33. doi:10.1093/gerona/50A.1.B26
Askew, G. N. and Marsh, R. L. (1997). The effects of length trajectory on the mechanical power output of mouse skeletal muscle. *J. Exp. Biol.* **200**, 3119-3131. doi:10.1242/jeb.200.24.3119
Askew, G. N. and Marsh, R. L. (1998). Optimal shortening velocity (V/V_{max}) of skeletal muscle during cyclical contractions: length-force effects and velocity-dependent activation and deactivation. *J. Exp. Biol.* **201**, 1527-1540. doi:10.1242/jeb.201.10.1527
Azizi, E. and Roberts, T. J. (2014). Geared up to stretch: pennate muscle behavior during active lengthening. *J. Exp. Biol.* **217**, 376-381. doi:10.1242/jeb.094383
Azizi, E. and Roberts, T. J. (2010). Muscle performance during frog jumping: influence of elasticity on muscle operating lengths. *Proc. R. Soc. B* **277**, 1523-1530. doi:10.1098/rspb.2009.2051
Biewener, A. A., Corning, W. R. and Tobalske, B. W. (1998a). In vivo pectoralis muscle force-length behavior during level flight in pigeons (*Columbia livia*). *J. Exp. Biol.* **201**, 3293-3307. doi:10.1242/jeb.201.24.3293
Biewener, A. A., Koniezynski, D. D. and Baudinett, R. V. (1998b). In vivo muscle force-length behavior during steady-speed hopping in tammar wallabies. *J. Exp. Biol.* **201**, 1681-1694. doi:10.1242/jeb.201.11.1681
Biewener, A. A., Wakeling, J. M., Lee, S. S. and Arnold, A. S. (2014). Validation of Hill-type muscle models in relation to neuromuscular recruitment and force-velocity properties: predicting patterns of in vivo muscle force. *Integr. Comp. Biol.* **54**, 1072-1083. doi:10.1093/icb/icu070
Blix, M. (1894). Die lange und die spannung des muskels. *Skand Arch. Physiol.* **5**, 150-206. doi:10.1111/j.1748-1716.1894.tb00198.x
Bohm, S., Mersmann, F., Santuz, A. and Arampatzis, A. (2019). The force-length-velocity potential of the human soleus muscle is related to the energetic cost of running. *Proc. R. Soc. B* **286**, 20192560. doi:10.1098/rspb.2019.2560
Burkholder, T. J. and Lieber, R. L. (2001). Sarcomere length operating range of vertebrate muscles during movement. *J. Exp. Biol.* **204**, 1529-1536. doi:10.1242/jeb.204.9.1529
Caiozzo, V. J. (2002). Plasticity of skeletal muscle phenotype: mechanical consequences. *Muscle Nerve* **26**, 740-768. doi:10.1002/mus.10271
Chow, J. W. and Darling, W. G. (1999). The maximum shortening velocity of muscle should be scaled with activation. *J. Appl. Physiol.* **86**, 1025-1031. doi:10.1152/jappl.1999.86.3.1025
Cox, S. M., Easton, K. L., Lear, M. C., Marsh, R. L., Delp, S. L. and Rubenson, J. (2019). The interaction of compliance and activation on the force-length operating range and force generating capacity of skeletal muscle: a computational study using a guinea fowl musculoskeletal model. *Integr. Org. Biol.* **1**, obz022. doi:10.1093/iob/obz022
Daley, M. A. and Biewener, A. A. (2003). Muscle force-length dynamics during level *versus* incline locomotion: a comparison of *in vivo* performance of two guinea fowl ankle extensors. *J. Exp. Biol.* **206**, 2941-2958. doi:10.1242/jeb.00503
Daley, M. A. and Biewener, A. A. (2011). Leg muscles that mediate stability: mechanics and control of two distal extensor muscles during obstacle negotiation in the guinea fowl. *Proc. R. Soc. B* **366**, 2693-2707.
Daley, M. A., Felix, G. and Biewener, A. A. (2007). Running stability is enhanced by a proximo-distal gradient in joint neuromechanical control. *J. Exp. Biol.* **210**, 383-394. doi:10.1242/jeb.02668
Daley, M. A., Voloshina, A. and Biewener, A. A. (2009). The role of intrinsic muscle mechanics in the neuromuscular control of stable running in guinea fowl. *J. Physiol.* **587**, 2693-2707. doi:10.1113/jphysiol.2009.171017
De Haan, A. (1988). Comparison of force-velocity characteristics obtained using twitches and tetani from in situ rat skeletal muscles. *Q. J. Exp. Physiol.* **73**, 131-133. doi:10.1113/expphysiol.1988.sp003111
Delp, S. L., Anderson, F. C., Arnold, A. S., Loan, P., Habib, A., John, C. T., Guendelman, E. and Thelen, D. G. (2007). OpenSim: open-source software to create and analyze dynamic simulations of movement. *IEEE Trans. Biomed. Eng.* **54**, 1940-1950. doi:10.1109/TBME.2007.901024
Dick, T. J., Clemente, C. J., Punith, L. K. and Sawicki, G. S. (2021). Series elasticity facilitates safe plantar flexor muscle–tendon shock absorption during perturbed human hopping. *Proc. R. Soc. B* **288**, 20210201. doi:10.1098/rspb.2021.0201
Edman, K. A. P. (2012). Residual force enhancement after stretch in striated muscle. A consequence of increased myofilament overlap? *J. Physiol.* **590**, 1339-1345. doi:10.1113/jphysiol.2011.222729
Edman, K. A. P., Elzinga, G. and Noble, M. I. (1982). Residual force enhancement after stretch of contracting frog single muscle fibers. *J. Gen. Physiol.* **8**, 769-784. doi:10.1085/jgp.80.5.769
Fenn, W. O. and Marsh, B. S. (1935). Muscular force at different speeds of shortening. *J. Physiol.* **85**, 277-297. doi:10.1113/jphysiol.1935.sp003318
Gabaldón, A. M., Nelson, F. E. and Roberts, T. J. (2008). Relative shortening velocity in locomotor muscles: turkey ankle extensors operate at low V/Vmax. *Am. J. Physiol. Regul. Integr. Comp. Physiol.* **294**, R200-R210. doi:10.1152/ajpregu.00473.2007
Gordon, A. M., Huxley, A. F. and Julian, F. J. (1966). The variation in isometric tension with sarcomere length in vertebrate muscle fibres. *J. Physiol.* **184**, 170-192. doi:10.1113/jphysiol.1966.sp007909
Gordon, J. C., Holt, N. C., Biewener, A. A. and Daley, M. A. (2020). Tuning of feedforward control enables stable muscle force-length dynamics after loss of autogenic proprioceptive feedback. *Elife* **9**, e53908. doi:10.7554/eLife.53908
Gordon, J. C., Rankin, J. W. and Daley, M. A. (2015). How do treadmill speed and terrain visibility influence neuromuscular control of guinea fowl locomotion? *J. Exp. Biol.* **218**, 3010-3022. doi:10.1242/jeb.104646
Gregor, R. J., Roy, R. R., Whiting, W. C., Lovely, R. G., Hodgson, J. A. and Edgerton, V. R. (1988). Mechanical output of the cat soleus during treadmill locomotion: in vivo vs in situ characteristics. *J. Biomech.* **21**, 721-732. doi:10.1016/0021-9290(88)90281-3
Gregoire, L., Veeger, H. E., Huijling, P. A. and Van Ingen Schenau, G. J. (1984). Role of mono- and biarticular muscle in explosive movements. *Int. J. Sports Med.* **5**, 301-305. doi:10.1055/s-2008-1025921
Griffiths, R. I. (1989). The mechanics of the medial gastrocnemius muscle in the freely hopping wallaby (*Thylogale billardierii*). *J. Exp. Biol.* **147**, 439-456. doi:10.1242/jeb.147.1.439
Hahn, D. and Riedel, T. N. (2018). Residual force enhancement contributes to increased performance during stretch-shortening cycles of human plantor flexor muscles *in vivo*. *J. Biomech.* **77**, 190-193. doi:10.1016/j.jbiomech.2018.06.003
Herzog, W. (2018). The multiple roles of titin in muscle contraction and force production. *Biophys. Rev.* **10**, 1187-1199. doi:10.1007/s12551-017-0395-y
Herzog, W. (2019). Passive force enhancement in striated muscle. *J. Appl. Physiol.* **126**, 1782-1789. doi:10.1152/japplphysiol.00676.2018
Herzog, W., Leonard, T. R., Renaud, J. M., Wallace, J., Chaki, G. and Bornemisza, S. (1992). Force-Length properties and functional demands of cat gastrocnemius, soleus and plantaris muscles. *J. Biomech.* **25**, 1329-1335. doi:10.1016/0021-9290(92)90288-C
Hessel, A. L., Monroy, J. A. and Nishikawa, K. C. (2021). Non-cross bridge viscoelastice elements contribute to muscle force and work during stretch-shortening cycles: evidence from whole muscles and permeabilized fibers. *Front. Physiol.* **12**, 640819. doi:10.3389/fphys.2021.648019
Hill, A. V. (1938). The heat of shortening and the dynamic constants of muscle. *Proc. R. Soc. B* **126**, 136-195.
Holt, N. C. and Azizi, E. (2014). What drives activation dependent shifts in the force– length curve? *Biol. Lett.* **10**, 20140651. doi:10.1098/rsbl.2014.0651
Holt, N. C. and Azizi, E. (2016). The effect of activation level on muscle function during locomotion: are optimal lengths and velocities always used? *Proc. R. Soc. B* **283**, 20152832. doi:10.1098/rspb.2015.2832
Holt, N. C., Wakeling, J. M. and Biewener, A. A. (2014). The effect of fast and slow motor unit activation on whole-muscle mechanical performance: the size principle

may not pose a mechanical paradox. *Proc. R. Soc. B* **281**, 20140002. doi:10.1098/rspb.2014.0002
Huxley, H. E. (1957). The double array of filaments in cross-striated muscles. *J. Biophys. Biochem. Cytol.* **3**, 631-648. doi:10.1083/jcb.3.5.631
James, R. S., Cole, N. J., Davies, M. L. F. and Johnston, I. A. (1998). Scaling of intrinsic contractile properties and myofibrillar protein composition of fast muscle in the fish *Myoxocephalus scorpius* L. *J. Exp. Biol.* **201**, 901-912. doi:10.1242/jeb.201.7.901
Jones, D. A. (2010). Changes in the force-velocity relationship of fatigues muscle: implications for power production and possible causes. *J. Physiol.* **588**, 2977-2986. doi:10.1113/jphysiol.2010.190934
Josephson, R. K. (1985). Mechanical power output from striated muscle during cyclic contraction. *J. Exp. Biol.* **114**, 493-512. doi:10.1242/jeb.114.1.493
Josephson, R. K. (1999). Dissecting muscle power output. *J. Exp. Biol.* **202**, 3369-3375. doi:10.1242/jeb.202.23.3369
Joumaa, V., Rassier, D. E., Leonard, T. R. and Herzog, W. (2008). The origin of passive force enhancement in skeletal muscle. *Am. J. Physiol. Cell Physiol.* **294**, 74-78. doi:10.1152/ajpcell.00218.2007
Lappin, A. K., Monroy, J. A., Pilarski, J. Q., Zepnewski, E. D., Pierotti, D. J. and Nishikawa, K. C. (2006). Storage and recovery of elastic potential energy powers ballistic prey capture in toads. *J. Exp. Biol.* **209**, 2535-2553. doi:10.1242/jeb.02276
Lichtwark, G. A. and Wilson, A. M. (2006). Interactions between the human gastrocnemius muscle and the Achilles tendon during incline, level and decline locomotion. *J. Exp. Biol.* **209**, 4379-4388. doi:10.1242/jeb.02434
Lieber, R. L. and Ward, S. R. (2011). Skeletal muscle design to meet functional demands. *Philos. Trans. R. Soc. Lond. B Biol. Sci.* **366**, 1466-1476. doi:10.1098/rstb.2010.0316
Loeb, G. E., Brown, I. E. and Cheng, E. J. (1999). A hierarchical foundation for models of sensorimotor control. *Exp. Brain Res.* **126**, 1-18. doi:10.1007/s002210050712
Luiker, E. A. and Stevens, E. D. (1994). Effect of temperature and stimulus train duration on the departure from theoretical maximum work in fish muscle. *Can. J. Zool.* **72**, 965-969. doi:10.1139/z94-132
Mathis, A., Mamidanna, P., Cury, K. M., Abe, T., Murthy, V. N., Mathis, M. W. and Bethge, M. (2018). DeepLabCut: markerless pose estimation of user-defined body parts with deep learning. *Nat. Neurosci.* **21**, 1281-1289. doi:10.1038/s41593-018-0209-y
McGowan, C. P., Neptune, R. R. and Herzog, W. (2013). A phenomenological muscle model to assess history dependent effects in human movement. *J. Biomech.* **46**, 151-157. doi:10.1016/j.jbiomech.2012.10.034
Mendoza, E., Martinez, M., Olberding, J. P. and Azizi, E. (2023). The effects of temperature on elastic energy storage and release in a system with a dynamic mechanical advantage latch. *J. Exp. Biol.* **226**, jeb245805. doi:10.1242/jeb.245805
Naples, G. G., Mortimer, J. T., Scheiner, A. and Sweeney, J. D. (1988). A spiral nerve cuff electrode for peripheral nerve stimulation. *IEEE Trans. Biomed. Eng.* **35**, 905-916. doi:10.1109/10.8670
Nath, T., Mathis, A., Chen, A. C., Patel, A., Bethge, M. and Mathis, M. W. (2019). Using DeepLabCut for 3D markerless pose estimation across species and behaviors. *Nat. Protoc.* **14**, 2152-2176. doi:10.1038/s41596-019-0176-0
Nelson, F. E., Gabaldon, A. M. and Roberts, T. J. (2004). Force-velocity properties of two avian hindlimb muscles. *Comp. Biochem. Physiol. A Mol. Int. Phys.* **137**, 711-721. doi:10.1016/j.cbpb.2004.02.004
Perreault, E. J., Heckman, C. J. and Sandercock, T. G. (2003). Hill muscle model errors during movement are greatest within the physiologically relevant range of motor unit firing rates. *J. Biomech.* **36**, 211-218. doi:10.1016/S0021-9290(02)00332-9
Prilutsky, B. I., Herzog, W. and Allinger, T. L. (1996). Mechanical power and work of cat soleus, gastrocnemius and plantaris muscles during locomotion: possible functional significance of muscle design and force patterns. *J. Exp. Biol.* **4**, 801-814. doi:10.1242/jeb.199.4.801
Raj, I. S., Bird, S. R. and Shield, A. J. (2010). Aging and the force-velocity relationship of muscles. *Exp. Gerontol.* **45**, 81-90. doi:10.1016/j.exger.2009.10.013
Rassier, D. E., MacIntosh, B. R. and Herzog, W. (1999). Length dependence of active force production in skeletal muscle. *J. Appl. Physiol.* **86**, 1445-1457. doi:10.1152/jappl.1999.86.5.1445
Rice, N., Bemis, C. M., Daley, M. A. and Nishikawa, K. (2023). Understanding muscle function during perturbed *in vivo* locomotion using a muscle avatar approach. *J. Exp. Biol.* **226**, jeb244721. doi:10.1242/jeb.244721
Richards, C. T. and Eberhard, E. Z. (2020). *In vitro* virtual reality: an anatomically explicit musculoskeletal simulation powered by *in vitro* muscle using closed-loop tissue–software interaction. *J. Exp. Biol.* **223**, jeb210054. doi:10.1242/jeb.210054
Roberts, T. J. (2001). Muscle force and stress during running in dogs and wild turkeys. *Bull. Mus. Comp. Zool.* **156**, 283-295.
Roberts, T. J. and Konow, N. (2013). How tendons buffer energy dissipation by muscle. *Exerc. Sport Sci. Rev.* **41**, 186-193. doi:10.1097/JES.0b013e3182a4e6d5
Roberts, T. J., Marsh, R. L., Weyand, P. G. and Taylor, C. R. (1997). Muscular force in running turkeys: the economy of minimizing work. *Science* **275**, 1113-1115. doi:10.1126/science.275.5303.1113
Robertson, B. D. and Sawicki, G. S. (2015). Unconstrained muscle-tendon workloops indicate resonance tuning as a mechanism for elastic limb behavior during terrestrial locomotion. *Proc. Nat. Acad. Sci. USA* **112**, E5891-E5898. doi:10.1073/pnas.1500702112
Rome, L. C. (1998). Some advances in integrative muscle physiology. *Comp. Biochem. Physiol. B Biochem. Mol. Biol.* **120**, 51–72.
Rome, L. C. and Lindstedt, S. L. (1997). Mechanical and metabolic design of the muscular system in vertebrates. In *Handbook of Physiology* (ed. W. H. Dantzler), pp. 1587-1652. Bethesda, MD: American Physiological Society.
Rubenson, J., Pires, N. J., Loi, H. O., Pinniger, G. J. and Shannon, D. G. (2012). On the ascent: the soleus operating length is conserved to the ascending limb of the force-length curve across gait mechanics in humans. *J. Exp. Biol.* **215**, 3539-3551. doi:10.1242/jeb.070466
Sawicki, G. S., Robertson, B. D., Azizi, E. and Roberts, T. J. (2015). Timing matters: tuning the mechanics of a muscle–tendon unit by adjusting stimulation phase during cyclic contractions. *J. Exp. Biol.* **218**, 3150-3159. doi:10.1242/jeb.121673
Schwaner, M. J., Lin, D. C. and McGowan, C. P. (2018). Jumping mechanics of desert kangaroo rats. *J. Exp. Biol.* **221**, jeb186700. doi:10.1242/jeb.186700
Schwaner, M. J., Lin, D. C. and McGowan, C. P. (2021). Plantar flexor muscles of kangaroo rats (*Dipodomys deserti*) shorten at a velocity to produce optimal power during jumping. *J. Exp. Biol.* **224**, jeb242630. doi:10.1242/jeb.242630
Schwaner, M. J., Nishikawa, K. C. and Daley, M. A. (2022). Kinematic trajectories in response to speed perturbations in walking suggest modular task-level control of leg angle and length. *Integr. Comp. Biol.* icac057. doi:10.1093/icb/icac057
Schwaner, M. J., Gordon, J. C., Biewener, A. A. and Daley, M. A. (2023). Muscle force–length dynamics during walking over obstacles indicates delayed recovery and a shift towards more 'strut-like' function in birds with proprioceptive deficit. *J. Exp. Biol.* **226**, jeb245199. doi:10.1242/jeb.245199
Schwaner, M. J., Mayfield, D. L., Azizi, E. and Daley, M. A. (2024). Data from: Linking *in vivo* muscle dynamics to in situ force-length and force-velocity reveals that guinea fowl lateral gastrocnemius operates at shorter than optimal lengths [Dataset]. Dryad. https://doi.org/10.5061/dryad.0p2ngf26p
Seiberl, W., Power, G. A., Herzog, W. and Hahn, D. (2015). The stretch-shortening cycle (ssc) revised: residual force enhancement contributes to increased performance during fast sscs of human m. adductor pollicis. *Phys. Rep.* **3**, e12401.
Seth, A., Hicks, J. L., Uchida, T. K., Habib, A., Dembia, C. L., Dunne, J. J., Ong, C. F., DeMers, M. S., Rajagopal, A., Millard, M. et al. (2018). OpenSim: Simulating musculoskeletal dynamics and neuromuscular control to study human and animal movement. *PLoS Comput. Biol.* **14**, e1006223. doi:10.1371/journal.pcbi.1006223
Sponberg, S., Abbott, E. and Sawicki, G. S. (2023). Perturbing the muscle work loop paradigm to unravel the neuromechanics of unsteady locomotion. *J. Exp. Biol.* **226**, jeb243561. doi:10.1242/jeb.243561
Stevens, E. D. (1996). The pattern of stimulation influences the amount of oscillatory work done by frog muscle. *J. Physiol.* **494**, 279-285. doi:10.1113/jphysiol.1996.sp021490
Strojnik, V. (1995). Muscle activation level during maximal voluntary effort. *Eur. J. App. Physiol. Occ. Ther.* **72**, 144-149. doi:10.1007/BF00964129
Sugi, H. and Ohno, T. (2019). Physiological significance of the force-velocity relation in skeletal muscle and muscle fibers. *Int. J. Mol. Sci.* **20**, 3075. doi:10.3390/ijms20123075
Tu, M. S. and Dickinson, M. H. (1994). Modulation of negative work output from a steering muscle of the blowfly *Calliphora vicina*. *J. Exp. Biol.* **192**, 207-224. doi:10.1242/jeb.192.1.207
Von Tscharner, V. (2000). Intensity analysis in time-frequency space of surface myoelectric signals by wavelets of specified resolution. *J. Electromyogr. Kinesiol.* **10**, 433-445. doi:10.1016/S1050-6411(00)00030-4
Wakeling, J. M., Kaya, M., Temple, G. K., Johnston, I. A. and Herzog, W. (2002). Determining patterns of motor recruitment during locomotion. *J. Exp. Biol.* **205**, 359-369. doi:10.1242/jeb.205.3.359
Walmsley, B., Hodgson, J. A. and Burke, R. E. (1978). Force produced by medial gastrocnemius and soleus muscles during locomotion in freely moving cats. *J Neurophys* **41**, 1203-1216. doi:10.1152/jn.1978.41.5.1203
Zajac, F. E. (1989). Muscle and tendon: properties, models, scaling, and application to biomechanics and motor control. *Crit. Rev. Biomed. Eng.* **17**, 359-411.
Zajac, F. E., Neptune, R. R. and Kautz, S. A. (2002). Biomechanics and muscle coordination of human walking. Part I: Introduction to concepts, power transfer, dynamics and simulations. *Gait Posture* **16**, 215-232. doi:10.1016/S0966-6362(02)00068-1
Zajac, F. E., Neptune, R. R. and Kautz, S. A. (2003). Biomechanics and muscle coordination of human walking: part II: lessons from dynamical simulations and clinical implications. *Gait Posture* **17**, 1-17. doi:10.1016/S0966-6362(02)00069-3

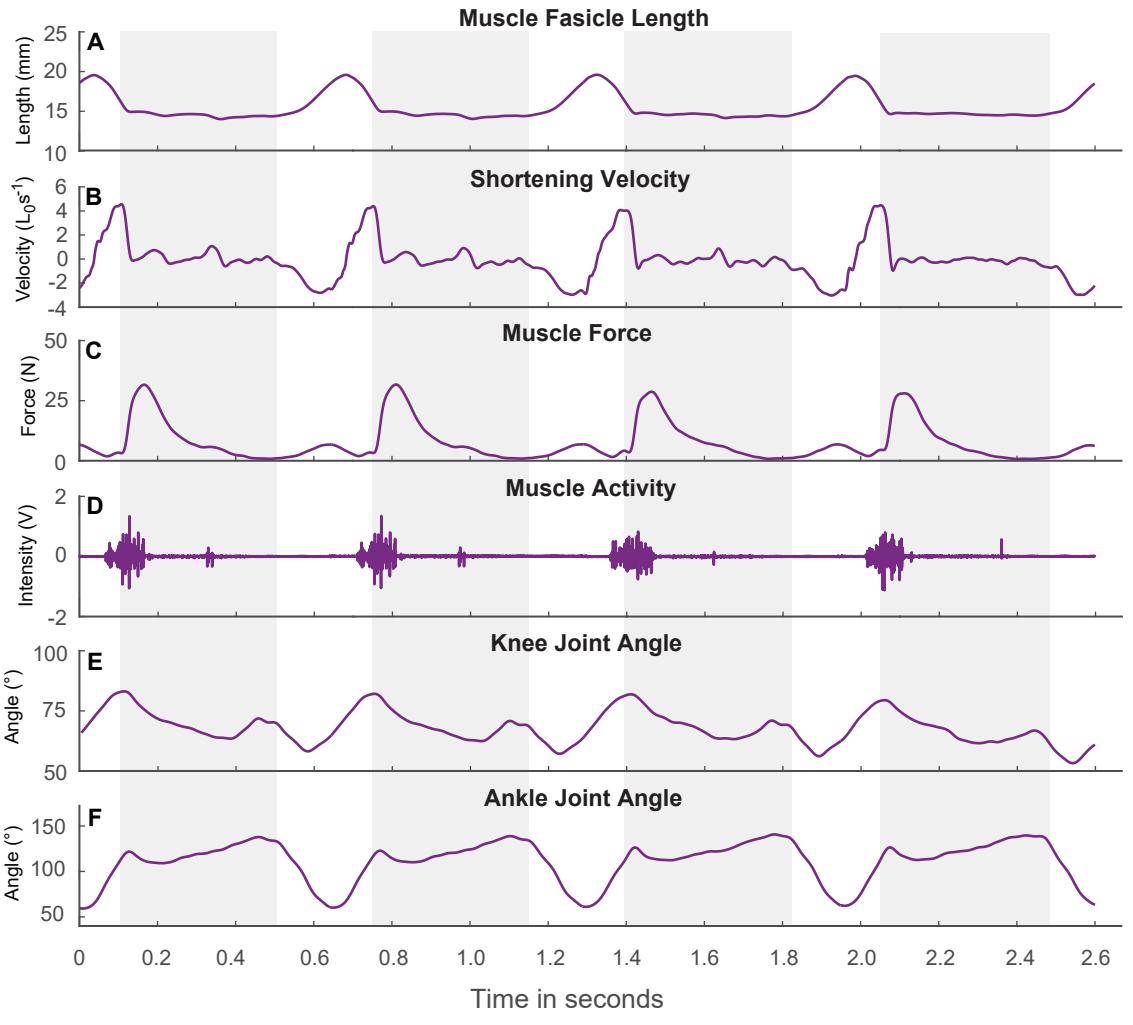

Fig. S1. Muscle dynamics and joint kinematics of 4 consecutive strides during walking. Muscle fascicle length in millimeters (A), muscle fascicle shortening velocity in $L0s^{-1}$(B), LG muscle tendon force in Newton (C), muscle activation (D), and knee (E) and ankle (F) joint angles in degrees, are presented for 4 consecutive strides for a bird (Ind3) during steady walking on the treadmill. Muscle activation data presented here is the raw EMG data, before filters are applied.

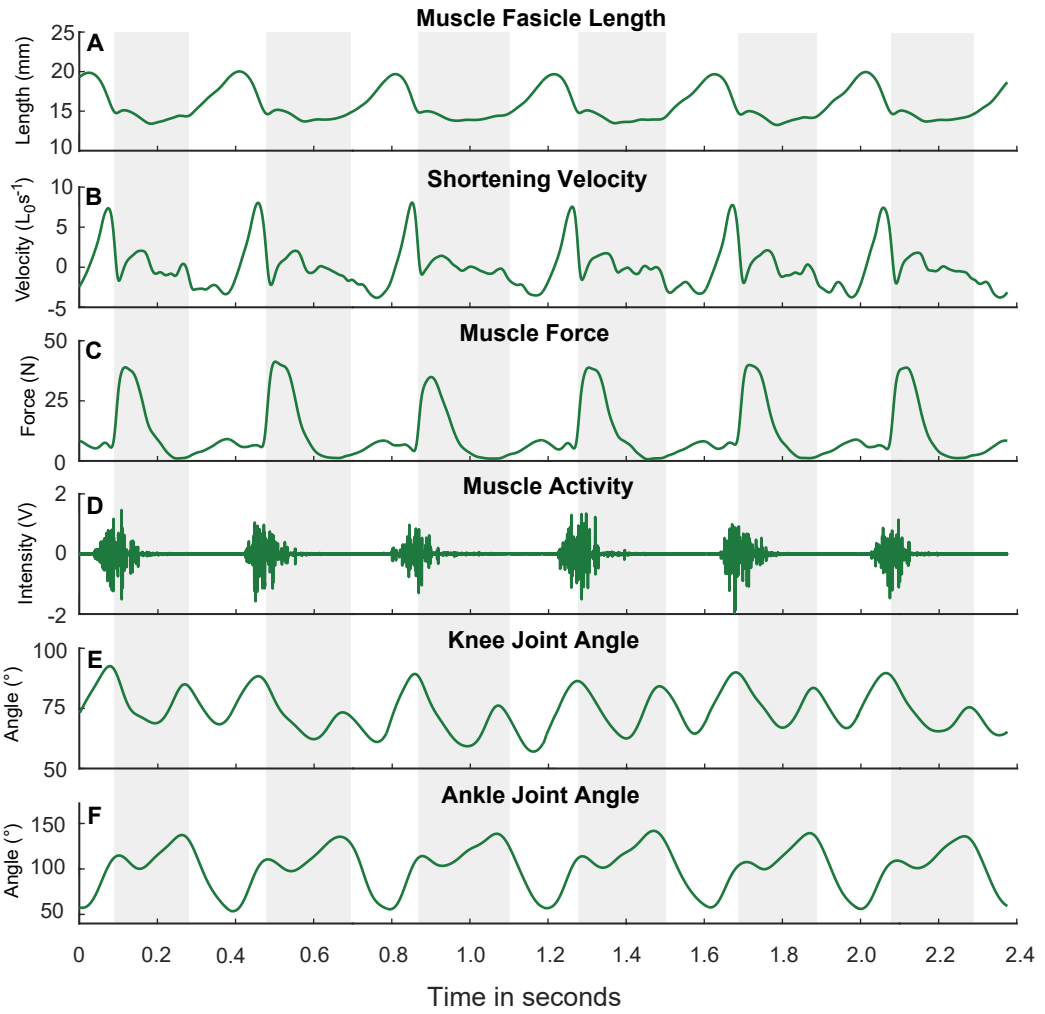

Fig. S2. Muscle dynamics and joint kinematics of 6 consecutive strides during running. Muscle fascicle length in millimeters (A), muscle fascicle shortening velocity in $L0s^{-1}$ (B), LG muscle tendon force in Newton (C), muscle activation (D), and knee (E) and ankle (F) joint angles in degrees, are presented for 6 consecutive strides for a bird (Ind3) during steady running on the treadmill. Muscle activation data presented here is the raw EMG data, before filters are applied.

Table S1. Morphological measurement. For each measurement we present the average ± 1 standard deviation (SD), for n = 11 individuals.

	Average ± SD
LG mass (g)	9.7 ± 1.1
MG mass (g)	14.0 ± 1.3
LG PCSA (mm^2)	475 ± 61
Gastroc PCSA (mm^2)	1163 ± 106
Pinnation Angle (°)	22.0 ± 4.0
LG Fascicle length, L_f (mm)	22.3 ± 1.0
LG belly length (mm)	98.8 ± 7.3
LG thickness (mm)	10.1 ± 1.4

Table S2. Measured free-tendon length from muscle-tendon junction to clamp *versus* force, length, and velocity measures. We report the free tendon length within the in situ preparation, measured from the muscle tendon junction to the clamp, as well as the fascicle shortening during the maximum tetanic fixed-end isometric contraction (ΔL) (equal to total tendon strain, because total length change is zero). We also report the maximum isometric force (F_{max}), the effective stiffness, the strain width of the F-L plateau (as a fraction of L_0), and the measured optimal shortening velocity (V_{opt}). For each measurement we report the value for each individual and the mean and standard deviation across individuals. Lastly, we report the correlation coefficient (r) and R^2, with the free-tendon length (from muscle-tendon junction to clamp) as the predictor. In our in situ preparations there was substantial variation in free tendon length, but it does not appear to be the main predictor of the individual variation in measured F-L and F-V characteristics (Supplemental Table 2). The relatively consistent compliance despite variation in free tendon length suggests that most of the tendon compliance occurs in the aponeurosis.

ID #	**Tendon Length (mm)** [MT junction - clamp]	**ΔL (mm)**		**F_{max} (N)**		**Stiffness (N/mm)**		**Strain Width (L_0)**		**V_{opt} (L_0 s^{-1})**	
1	11.69	4.05		142.87		32.91		0.33		3.05	
2	15.92	5.97		101.39		17.02		0.34		3.39	
5	9.74	5.77		139.66		23.09		0.23		2.74	
6	23.72	11.78		193.57		20.57		0.39		3.10	
7	28.46	9.20		110.41		11.83		0.36		3.37	
12	25.45	6.30		139.17		21.15		0.27		3.57	
21	24.21	3.19		152.10		48.42		0.24		2.22	
22	29.81	5.48		136.93		23.83		0.28		2.69	
23	26.61	7.08		146.66		19.90		0.28		2.83	
24	16.41	5.56		125.49		22.99		0.26		2.66	
25	17.24	5.28		107.42		20.47		0.27		2.60	
Average ±SD	20.84 ± 6.58	6.33 ± 2.26		135.97 ± 24.38		23.84 ± 9.16		0.29 ± 0.05		2.93 ± 0.39	
		r	***R^2***	***r***	***R^2***	***r***	***R^2***	***r***	***R^2***	***r***	***R^2***
	Statistics	0.3632	0.1319	0.1846	0.03407	-0.1184	0.01402	0.284	0.0333	0.1	0.01

Table S3. Coefficients and fit parameters for the Force-Length and Force-Velocity curves across birds. For the FL and FV curve the fitted coefficients (a, b, c), number of datapoints fitted, and the R-squared (R^2) are reported.

	Force-Length relationship					**Force-Velocity relationship**				
	$y = a\,x^2 + b\,x + c$			fit parameters		$y = a + b\,/\,(x + c)$			fit parameters	
ID #	*a*	*b*	*c*	*data points*	R^2	*a*	*b*	*c*	*data points*	R^2
1	-0.587	24.740	-117.658	9	0.737	-0.931	10.557	5.443	7	0.997
2	-0.468	18.235	-76.300	11	0.930	-0.563	6.110	3.647	7	0.993
5	-1.769	62.500	-412.411	11	0.629	-0.884	7.897	4.015	7	0.994
6	-0.740	27.655	-64.773	8	0.989	-1.939	29.725	10.618	11	0.945
7	-0.442	17.373	-60.493	7	0.901	-0.539	5.705	3.232	7	0.999
12	-1.115	41.671	-250.282	11	0.888	-1.013	12.538	6.226	8	0.994
21	-0.588	24.633	-182.151	8	0.806	-0.634	4.759	2.696	7	0.995
22	-1.002	39.099	-244.446	8	0.812	-0.847	8.062	4.630	8	0.992
23	-0.770	33.922	-226.480	9	0.793	-1.706	28.042	10.830	8	0.999
24	-0.983	37.557	-233.432	10	0.780	-0.814	8.479	5.162	10	0.997
25	-0.638	26.625	-170.446	8	0.880	-0.344	3.021	1.752	12	0.934